UCRL- 95370
PREPRINT

Low Energy Neutron Capture of Neutron Rich Target Nuclides

G. Reffo
M. Blann
T. Komoto
R. J. Howerton

This paper was prepared for submittal to
Nuclear Instruments and Methods

September 1986

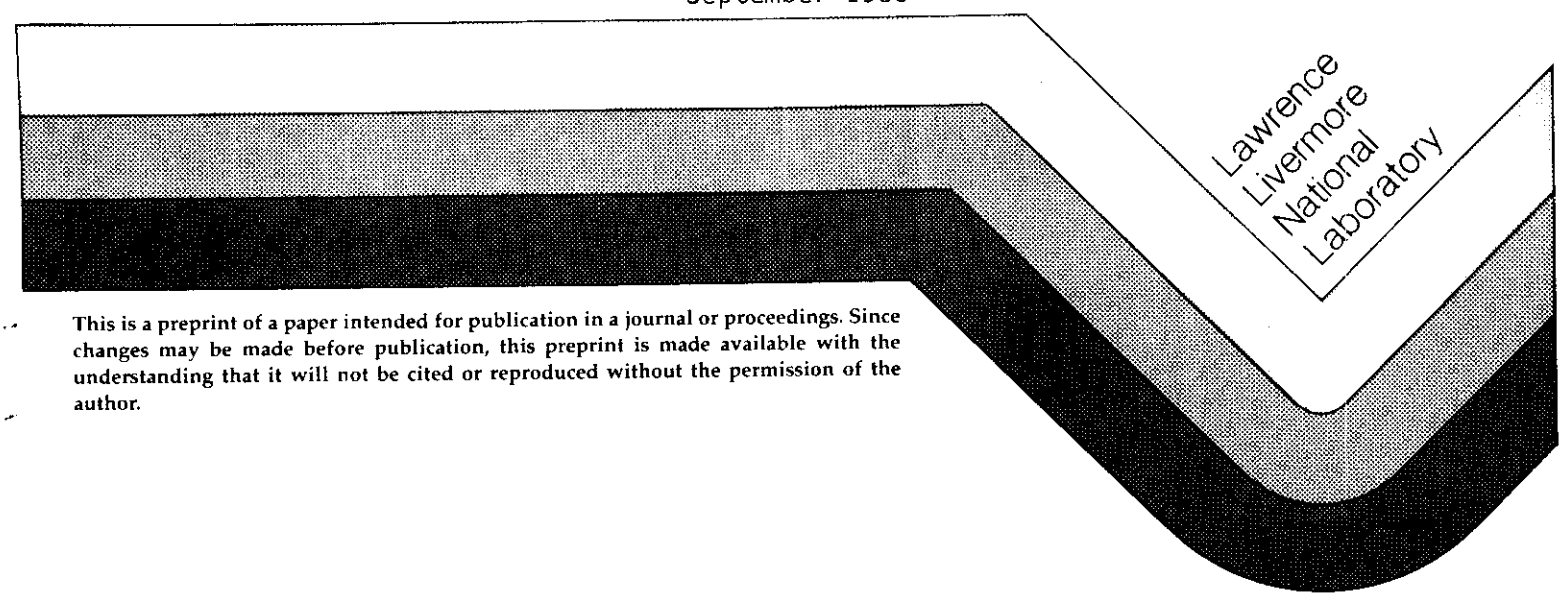

DISCLAIMER

LOW ENERGY NEUTRON CAPTURE

OF NEUTRON RICH TARGET NUCLIDES

Gianni Reffo
ENEA, Bologna, Italy
and E-Division, Physics Department
Lawrence Livermore National Laboratory

H. M. Blann, T. Komoto and R. J. Howerton
Physics Department
Lawrence Livermore National Laboratory

Abstract: We have used nuclear model codes developed at ENEA, Bologna, Italy, to calculate (n,γ) capture cross sections on 76 neutron-rich nuclides. The physics models used and the method of obtaining relevant input parameters are summarized.

Introduction: We have recently considered the question of calculating (n,γ) capture cross sections for very neutron rich nuclides for which no experimental measurements can be made. In this report, we summarize the physics models used for these calculations as contained in a system of computer codes written at ENEA, Bologna, Italy. These codes were formally used for calculation of cross sections for materials employed in the design of the Super Phoenix reactor. We discuss the systematics used to generate input parameters to these calculations and present results for 76 neutron rich nuclides. We also estimate uncertainties in the calculations for individual nuclides, and suggest steps which should be taken if a higher degree of accuracy is desired.

A. THEORETICAL APPROACH

A.1 The Cross Section Formalism

Hauser-Feshbach theory for particle capture cross sections yields:

$$\langle \sigma_{n\gamma}(E_n) \rangle = \frac{\pi \lambda^2}{(2s+1)(2I+1)} \sum_{\pi \ell j} (2J+1) t_{\ell j}^{J\pi} \qquad \text{(Eq. 1)}$$

$$\frac{T_\gamma^{J\pi}(E_n+B_n)}{\sum_{L\ell'j'} T_{\ell'j'}^{J\pi}(E_n-E_L) + T_\gamma^{J\pi}(E_n+B_n)} W_{\ell j \ell' j'}^{J\pi}(E) \quad ,$$

where s = incident particle spin, I = target spin, $\vec{j}=\vec{\ell}+\vec{s}$, J=total angular momentum, $t_\ell^{J\pi}(E)$ are the generalized optical model transmission coefficients, $W_{\ell j \ell' j'}^{J\pi}(E)$ is the width fluctuation correction factor (See Refs. RE-76, GR-77, RE-78), L = index labeling target levels, E_L = energy of L-th level, and $T_\gamma^{J\pi}$ the γ transmissions coefficients:

$$T_\gamma^{J\pi}(E_n+B_n) = \frac{2\pi\, \Gamma_\gamma^{J\pi}(E_n+B_n)}{D^{J\pi}(E_n+B_n)} \quad , \qquad \text{(Eq. 2)}$$

where $\Gamma_\gamma^{J\pi}(E_n+B_n)$ is the total γ-decay width of compound nucleus states of spin J and parity π at an excitation E_n+B_n (where B_n is the incident particle binding energy) and $D^{J\pi}(E_n+B_n)$ is the spacing of such states.

A.2 The γ-Decay Model

For the γ-decay description, the Brink-Axel hypothesis has been adopted. This consists of replacing the inverse process cross section (γ-absorption) by the Lorentzian fit of photon absorption cross sections. The cross section for the absorption of one photon of electric E (or magnetic M) character and of multipole order ℓ by an initial level i to a final single isolated level f is:

$$\sigma^{E(M),\ell}_{(i\to f)} = 2\pi\lambda^2 g \; \frac{\epsilon^2 \, \Gamma_\gamma^{E(M),\ell}(f\to i)\Gamma_f}{(\epsilon^2 - E_f^2)^2 + \epsilon^2 \Gamma_f^2} \quad , \qquad \text{(Eq. 3)}$$

where i and f denote also the quantum numbers of the initial and final levels (E_i, J_i, π_i) and (E_f, J_f, π_f) respectively.

$\epsilon = E_f - E_i$ is the photon energy

$\lambda = \frac{\hbar c}{\epsilon}$ is the photon wavelength

$g = \frac{2J_f+1}{2J_i+1}$ is a statistical factor

$\Gamma_\gamma^{E(M),\ell}(f\to i)$ is the partial width for the inverse process of de-excitation of the level f via a photon emission of electric E or magnetic M character and multipole order ℓ. Γ_f is the total width of the resonance (E_f, J_f, π_f).

The cross section integrated over the whole range containing the resonance (E_f, J_f, π_f) is:

$$I(i,f) = \int \sigma^{E(M),\ell}(i \to f)\, d\varepsilon = \pi^2 \lambda^2 g \Gamma_\gamma^{E(M),\ell}(f \to i) \quad . \qquad \text{(Eq. 4)}$$

By way of definition, the cross section averaged over a photon energy interval containing n resonances all characterized by the same spin and parity, as for f, is:

$$\langle \sigma^{E(M),\ell}(i \to f) \rangle_{\Delta\varepsilon} = \frac{\sum_1^n I_r(i,f)}{\Delta\varepsilon} \quad , \qquad \text{(Eq. 5)}$$

while the integrated cross section I(i,f) averaged in the same interval $\Delta\varepsilon$ is:

$$\langle I(i,f) \rangle_{\Delta\varepsilon} = \frac{\sum_1^n I_r(i,f)}{n} \qquad \text{(Eq. 6)}$$

We thus have:

$$\langle \sigma^{E(M),\ell}(i \to f) \rangle_{\Delta\varepsilon} = \frac{n}{\Delta\varepsilon} \langle I(i,f) \rangle_{\Delta\varepsilon} \quad , \qquad \text{(Eq. 7)}$$

where $\frac{\Delta\varepsilon}{n}$ is the mean spacing $D(E_f, J_f, \pi_f)$ of the resonances with spin J_f and parity π_f at the energy E_f, while:

$$\langle I(i,f) \rangle_{\Delta\varepsilon} = \pi^2 \lambda^2 g \langle \Gamma_\gamma^{E(M),\ell}(f \to i) \rangle_{\Delta\varepsilon} \quad . \qquad \text{(Eq. 8)}$$

By combining Eq. 7 and Eq. 8, one gets:

$$\langle\sigma^{E(M),\ell}(i\to f)\rangle_{\Delta\varepsilon} = \pi^2\lambda^2 g \langle\Gamma_\gamma^{E(M),\ell}(f\to i)\rangle_{\Delta\varepsilon} / D(E_f, J_f, \pi_f) \quad , \qquad \text{(Eq. 9)}$$

which relates the average radiative width for the transition (f→i) to the average photo cross section for the inverse absorption process (i→f). The Brink-Axel estimate is based on the result expressed by Eq. 9 in the light of the following assumptions:

1) Only electric dipole photo-absorption (E1) contributes to the excitation of the levels in the continuum energy region.

2) The average photo-absorption cross section is known and its energy dependence may be represented by a Lorentzian curve.

3) The average photo-absorption cross section does not depend on the initial state excitation energy.

Assumptions 1 and 2 are confirmed by the experimental evidence that the giant resonance is a general property of the ground state photo-absorption cross section which results primarily as built up from electric dipole absorption and its experimental shape is well described by one or more Lorentzian curves.

$$\sigma_\gamma(0,\varepsilon) = \sigma_L(\varepsilon) = \Sigma_R \sigma_R \frac{\varepsilon^2\Gamma_R^2}{(\varepsilon^2 - E_R^2)^2 + \varepsilon^2\Gamma_R^2} \quad , \qquad \text{(Eq. 10)}$$

where σ_R, E_R, Γ_R are fit parameters corresponding to the peak cross section, peak energy and half maximum width respectively.

As regards the absorption of photons by nuclei in an excited state in accordance with assumption 3, Rosenzweig (RO-68) has shown that there is some experimental evidence for the mean energy of the dipole strength distribution built on an excited state of energy E_i (relative to the ground state) being displaced upwards in energy by an amount E_i. This fact supports the idea that the total photo-absorption cross section built up on an excited state E_i with one photon of energy ε is related to the ground state photo-absorption by the equation:

$$\sigma(E_i \rightarrow E_f) = \sigma(0 \rightarrow E_f - E_i) \qquad \text{(Eq. 11)}$$

$E_f = E_i + \varepsilon$ being the excitation energy of the final state. According to this hypothesis, summation of Eq. 9 over all final states f related to the initial state i by E1 selection rules gives the equation:

$$\sigma_L(\varepsilon) = \pi^2 \lambda^2 \sum_f g \langle \Gamma_\gamma^{E1}(f \rightarrow i) \rangle_{\Delta\varepsilon} / D(E_f, J_f, \pi_f) \qquad \text{(Eq. 12)}$$

In addition, if the assumption is made that the radiative strength function $\langle \Gamma_\gamma^{E1}(f \rightarrow i) \rangle_{\Delta\varepsilon} / D(E_f, J_f, \pi_f)$ does not depend on J_f, the average radiative width for the transition (f→i) may be written as:

$$\langle \Gamma_\gamma^{E1}(f \rightarrow i) \rangle_{\Delta\varepsilon} = \varepsilon^2 \sigma_L(\varepsilon) D(E_f, J_f, \pi_f) / 3(\pi \hbar c)^2 \qquad \text{(Eq. 13)}$$

The total radiative width is obtained by summation of Eq. 13 over all the lower states i permitted by the E1 selection rules:

$$\bar{\Gamma}_\gamma(E_f,J_f,\pi_f) = \sum_i \langle \Gamma_\gamma^{E1}(f\to i)\rangle_{\Delta\varepsilon} \qquad \text{(Eq. 14)}$$

We split the summation in Eq. 14 into two parts to account for the transitions to the discrete levels, as well as to the levels in the continuum:

$$\bar{\Gamma}_\gamma(E_f,J_f,\pi_f) = \frac{2}{3(\pi\hbar c)^2\rho(E_f,J_f)} \sum_i\sum_{J_i} \delta_{\pi_i,-\pi_f}(E_f-E_i)^2\sigma_L(E_f-E_i) +$$

$$+ \frac{1}{3(\pi\hbar c)^2\rho(E_f,J_f)} \int_0^{E_f-E_{cut}} \varepsilon^2\sigma_L(\varepsilon)\sum_j\rho(E_f-\varepsilon,J)d\varepsilon \quad , \qquad \text{(Eq. 15)}$$

where E_i are the energies of the discrete levels.

A.3 The Level Density

The formulation for the level density $\rho(E,J,\pi)$ has been adopted from Gilbert and Cameron (GI-65):

$$\rho(E,J,\pi) = \begin{cases} \rho_1(E),f(J,E)p(\pi,E) & E<E_x \\ \rho_2(E)f(J,E)p(\pi,E) & E>E_x \end{cases} , \qquad \text{(Eq. 16)}$$

where f and p are the spin and parity energy dependent distribution laws $\rho_1(E)$ and $\rho_2(E)$ are the low and high energy total level density

expressions given by:

$$\rho_1(E) = \frac{1}{T} \; e^{(E-E_o)/T} \qquad \text{(Eq. 17)}$$

and

$$\rho_2(E) = \sqrt{\frac{\pi}{12}} \; \frac{\exp \; 2\sqrt{a(E-\Delta)}}{2\pi\sigma(E)a^{1/4}(E-\Delta)^{5/4}} \qquad \text{(Eq. 18)}$$

In Eqs. 18, Δ is the pairing energy. The two level-density formulae adopted are made to match at some excitation energy, E_x where:

$$\rho_1(E_x) = \rho_2(E_x) \qquad \text{(Eq. 19)}$$

and

$$\left.\frac{d\rho_1(E)}{dE}\right|_{E=E_x} = \left.\frac{d\rho_2(E)}{dE}\right|_{E=E_x} \qquad \text{(Eq. 20)}$$

Eq. 17 is phenomenological and is parameterized by fitting the discrete levels. Eq. 18 is derived from the Fermi gas model and is justified where the underlying statistical assumptions hold. The so-called level density parameter "a" in Eq. 18, even if it has a well known physical meaning and, in principle could be determined theoretically, (see Sect. B.2), in practice is taken as a free parameter. By assuming that Eq. 18 holds in the neutron reasonance region, "a" can be determined by fitting Eq. 18 to the mean spacing, $D_{observed}$, of neutron resonances,

$$\frac{1}{D_{OBS}} = 1/2 \sum_{J=|I-1/2|}^{I+1/2} \rho_2(E,J) \; . \qquad \text{(Eq. 21)}$$

Therefore, S-wave resonances are obviously most suited to this purpose. Let us designate the values of "a" so determined by "a^{EXP}". The normalization procedure expressed by Eq. 21 avoids obvious model approximations while assuring the validity of Eq. 18 in a broad neighborhood around the neutron binding energy B_n. As a matter of fact, fitting ρ_2 to the density of neutron resonances and ρ_1 to the density of discrete levels, one expects a reasonable reliability of the level density so determined in the whole energy range up to a few MeV above B_n, which is the region of main interest in low energy neutron capture.

The matching conditions (19) and (20) establish relationships among the various quantities involved in Eqs. 17 and 18. In particular, one has:

$$E_o = E_x - T[\ln \rho_2 (E_x)] \qquad \text{(Eq. 22)}$$

$$\frac{1}{T} = \sqrt{\frac{a}{U_x}} - \frac{3}{2U_x} \qquad \text{(Eq. 23)}$$

Equations (22) and (23) allow for a complete parametrization of the presently adopted level density by knowledge of only two parameters, "a" and either T or U_x, one for each of the two equations involved. T has the meaning of nuclear temperature, which has proven to be fairly constant in the low excitation energy region, in particular in the discrete level region. One advantage of the approach outlined is that the parameters involved, a, U_x and T, exhibit well established systematic trends.

B. PARAMETRIZATION

In order to obtain cross section values from Eq. 1, the following sets of parameters are necessary:

1. Optical model parameters (OMP)
2. Level density parameters (LDP)
3. γ-decay parameters (GRP)
4. Level schemes
5. Reaction q-values
6. Deformation parameters

B.1 Choice of Optical Model Parameters

The potential scattering radius, R, is related to the shape elastic cross section. Far from the resonance region $\sigma_{\text{shape elastic}} = 4\pi R^2$. This R contributes important information in selecting the real potential well depth. The strength functions, $S_{\ell=0}$, $S_{\ell=1}$, $S_{\ell=2}$, giving the magnitude of the average neutron absorption in the resonance region, are also useful in determinating the imaginary part of the potential. Because the incident energy range of interest here falls into or is very close to the neutron resonance region, it is appropriate to consider the quantities R, $S_{\ell=0}$, $S_{\ell=1}$, $S_{\ell=2}$, when choosing our OMP. Given the large uncertainties affecting parameters involved in our calculations, it is assumed that the average nucleon-nucleus interaction depends mainly only on A. Accordingly, reaction characteristics such as scattering radius R, strength functions S_ℓ, etc., also are assumed to depend only upon the target mass A. Within

such an approximation, the validity of R and S_ℓ systematics, as well as those of global OMP sets have been extrapolated off the stability valley. Among various global OMP sets available in the literature, we adopted Moldauer's (MO-83) spherical OMP set. In fact, this was determined by fitting the quantities R, $S_{\ell=0}$, $S_{\ell=1}$, and therefore, it seems especially suited to the energy region of interest here. For some of the isotopes involved in the present calculations sizeable direct collective contributions are expected. However, using coupled channel calculations would not improve the accuracy of the final result. In fact, in many cases, even the target ground state spin and parity are not known, while large uncertainties affect most of the other parameters. In Figs. 1 through 4, the results obtained with Moldauer's OMP are compared to the systematics of Mughabghab (MU-84) including coupled channels calculations, for s-,p-,d-wave strength functions and scattering radii respectively. The rather low values obtained for S_2 do not bother us much at the energies of interest here, but indicate that Moldauer's OMP should not be used at incident energies much higher than the resonance region, where higher order ℓ-values are involved.

B.2 Level Density

B.2.1 Level Density Parametrization

According to the Fermi gas model, by way of definition (GI-65):

$$a = \frac{\pi^2}{6} g \qquad \text{and} \qquad g = \frac{\Delta N(\varepsilon)}{\Delta \varepsilon}\bigg|_{\varepsilon = E_F} \qquad \text{(Eq. 24)}$$

where $N(\varepsilon)$ = cumulative number of single particle states, E_F = the energy of the Fermi level with $\Delta\varepsilon$ an energy interval around the Fermi level of the order of the thermodynamic temperature t, where the density of single particle states g has to be determined. In Fig. 5, g is shown as obtained from Eq. 24 in terms of the unified Nilsson model for different deformation parameters β for a thermodynamical temperature typical of neutron resonances. In Fig. 5, one observes that for low β-values (e.g. β=.1), the trend of the parameter g exhibits typical shell closure dips at magic neutron or proton numbers, whereas at increasing β-values this trend tends to disappear. Such a pattern, besides a dependence on β, also indicates a dependence on N and Z according to different single particle state spectra typical of different nuclei. So it appears convenient to plot experimental values of "a" as deduced from neutron resonance spacings vs. N to give overall systematics, as shown in Fig. 6. If in addition, "a"-values are grouped according to isotope-families, one gets local systematics where the Z- and β-dependence are simultaneously accounted for as well.

In a statistical sense, Eq. 24 implies that the nucleons participating in the excitation process are those lying in the orbitals within the mentioned interval $\Delta\varepsilon \sim t$ around the Fermi top. Because t depends on the excitation energy E then it is $a=a(E)$. According to such a picture, a(E) is expected to behave asymptotically with E. In fact, for low E-values, a(E) is fluctuating with E according to the single particle state spectrum typical of the nucleus considered. At increasing E, $\Delta\varepsilon$ includes an increasing number of single particle states so that the derivative in Eq. 24 becomes more and more independent of $\Delta\varepsilon$ while approaching its asymptotic value. Because t behaves like the square root of E, "a" varies slowly with E within small intervals of E-values, but not for E-values too low. This conclusion and the assumption

that neutron binding energies are high enough, underlie the approximation that "a" is energy independent, which we used in deriving our systematics. The latter were obtained, according to Eq. 21, from mean observed spacing, D_{OBS}, of neutron resonances because these constitute the largest source of experimental information useful to this end.

In practice, neutron resonances are available only for stable nuclei where B_n ranges (except for a few cases) over a fairly narrow interval of values around 7 MeV. Therefore what one obtains are the systematics of "a" at B_n. In general, B_n is below the excitation energy region where "a" reaches its asymptotic value even if $a(B_n)$ can be close to it. To the extent that B_n is low and $a(B_n)$ is far from its asymptotic value, one has to expect some consequent spread in "a"-systematics. From this discussion, it should be clear that extrapolations of "a"-systematics off the stability valley are better justified for isotopes with a binding energy not much lower than ~6-7 MeV.

In Fig. 7, the systematics of the nuclear temperature vs mass number A do not exhibit any particular shell structure effect and show only a weak A-dependence. This behavior can be interpreted from the observation that the density of low lying discrete levels of all nuclei can be described by a constant nuclear temperature. This implies that, in the low energy range with increasing excitation, the energy distribution in the excited system does not change appreciably. As far as this picture is realistic, one expects that the trend of the nuclear temperature should depend only on A regardless of shell closure effects, as can be seen in Fig. 7 and of the location with respect to the valley of β stability. Due to the very slow variation of T with A, U_x also shows a well established trend (see Fig. 7) according to the correlation with "a" as expressed in Eq. 23.

The methods outlined and discussed for systematizing the level density parameters have been used extensively in the stability valley region and have proven satisfactory and reliable.

In order to derive local systematics, best suited to extrapolations for the purposes of the present work, we have considered all available experimental information on discrete level schemes (see Sec. D) and on neutron resonance schemes (MU-84) for all isotopes of all families of interest. From analysis of this information, local systematics of a, U_x, T were deduced for each isotope family (see Figs. 8 and 9). Because no resonance schemes were available for unstable isotopes, determination of a^{EXP} was limited to stable isotopes only. Therefore, local systematics for "a" were extrapolated (see Figs. 8 and 9) according to the guidelines of the overall systematics in Fig. 6 and of the definition in Eq. 24 applied to Nilsson model orbitals, as given in Fig. 5. Discrete level schemes were available for a few unstable isotopes. For these, U_x and T parameters could be determined which clearly confirmed the reliability of the adopted extrapolations. Through Eq. 23, this also resulted in an indirect test on the local systematics adopted for "a" parameters. In the worst cases of very low B_n, the greater confidence in T systematics lead us to parametrize the level density based mostly on consideration on T. This procedure is fully justified in such cases, because $U_x > B_n+E_n$ (our neutron incident energies being $E_n \leq 500$ keV), and therefore the constant nuclear temperature approach ρ_1 would be used in any case over the entire energy range.

B.2.2 The Spin Distribution

According to GI-65 and RF-78, the following energy dependent spin distribution was adopted.

$$f(J,E) = \frac{(2J+1)e^{-(J+1/2)^2/2\sigma^2(E)}}{2\sigma^2(E)} \qquad \text{(Eq. 25)}$$

where

$$\sigma^2(E) = \begin{cases} = .146\sqrt{a(E-\Delta)}\ A^{2/3}, & \text{when } E \geq E_x \\ = \text{linear interpolation between } \sigma^2(E_x) \text{ and } \sigma^2_{LVL}, & \text{when } E_{cut} \leq E \leq E_x \end{cases}, \qquad \text{(Eq. 26)}$$

where A = mass number and E_{cut} is the energy of the first level of unknown J or π characteristics. σ^2_{LVL} is obtained by a maximum likelihood fit of the distribution law of Eq. 25 to the discrete level spin distribution. It is given by:

$$\sigma^2_{LVL} = \frac{1}{2L}\sum_{L'=1}^{L}(J_{L'}+1/2)^2 \qquad \text{(Eq. 27)}$$

where L = the maximum number of levels. The importance of using a correct spin distribution in γ-decay calculations is evident due to spin and parity selection rules of the γ-transitions. Less evident, but nonetheless very important, is the influence of the spin distribution on neutron capture due to the enhancement or suppression of the competition from certain neutron channels by way of total angular momentum conservation.

B.2.3 Parity Distribution

A parity distribution can be used of the form $p(E,\pi) = e^{a^{\pi}E+b^{\pi}}$ where a^{π}, b^{π} are fit parameters to the discrete level parity distribution, if available; if not, one has to assume $p(E,\pi) = 1/2$. Due to parity selection rules, the parity distribution plays an important role in γ-decay calculations.

B.3 Giant Resonance Parameter Systematics

For the E1 photon absorption cross section, $\sigma_L(\varepsilon)$ is given by the Lorentzian fit to the E1 photo-absorption cross section in the giant resonance region (see Eq. 10). Usually, R equals one or two; σ_R, Γ_R, ε_R are giant resonance characterisctics. The dependence on β of the giant resonance parameters is taken from the systematics of RF-78, see Figs. 10 and 11. Formula 15 and the adopted GRP parametrization have been shown (BE-74, RF-78) to give absolute values of the total radiative width of neutron resonances $\Gamma_{\gamma}^{J\pi}(B_n)$ provided the level density is correctly parametrized. They also proved to give satisfactory γ-ray spectra (WI-82, RE-83).

B.4 Discrete Level Schemes

Discrete level schemes were taken from ENSDF (Evaluated Nuclear Structure Data File). From the ENSDF file, an evaluated level scheme file was created from which level schemes could be directly read by the model codes CERBERO and AMLETO. Essentially, this was achieved by a few spin and parity assignments where strictly necessary, e.g., when J and π were not given for the ground state or where one had to choose among more than one possible spin assignment. In particular, for the ground state, spin and parity assignments were

made based on the Nilsson Model (given the deformation parameter) and based on systematic considerations of neighboring isotopes of similar even-odd characteristics. In the case of unknown level schemes, another very important piece of information is the energy of the first excited state E_1. In target nuclei, this determines the Q value of the neutron inelastic reaction and therefore plays a dominant role in the (n,γ) reaction as well. In compound nuclei, this also plays an important role because the placement of E_1 influences the total number of γ-ray transitions.

B.5 Mass Tables

Neutron binding energies are internally computed by the AMLETO and CERBERO codes. The data set is constituted by the atomic mass data tables of Wapstra and Bos (WA-77) and where these data are not available, by the theoretical calculations of Möller and Nix (MO-81).

B.6 Quadrupole Deformation Parameter β

The deformation parameter β is important in the present calculations. This is necessary information for shell model considerations about spin and parity assignments of ground states of unknown characteristics. Considerations of the systematics for the level density parameter "a" are also based on the shell model and on the dependence of "a" on β (see Fig. 7). In addition, however, β is used for determining the giant resonance parameters for which the absolute value and sign of β are necessary. In particular, the sign of β is more important because the relative size of the first and second photo absorption cross section peaks of the split giant resonance are

reversed depending upon the prolate and oblate shape of nuclei. This consequently affects the γ-decay probability.

The deformation parameters adopted and quoted in Table 1 were taken from Mö-81. An uncertainty $\Delta\beta = .05$ was estimated for all adopted values of β.

C. RESULTS

The information given by the resonance schemes was not always sufficient for the complete determination of local systematics of the level density parameter "a", even in the stability valley. In fact, for a large number of isotope families around the p-wave peaks, s- and p-wave resonances are mixed and cannot always be separated and identified. This makes the statistical analy- sis of resonance schemes difficult, if not impossible. For a number of iso- topes, only a few resonances are available so that statistical analysis is not very meaningful.

In order to determine the overall systematics of "a", sparse information can also be useful, but to determine local systematics for single isotope families a sufficient number of isotopes should be known for each family. Both to overcome the lack of reliable information and to check the results deduced from statistical analysis of neutron resonances, we had to refer to additional experimental information such as total radiative widths of neutron resonances $\Gamma_\gamma^{J\pi}(B_n)$ and neutron capture cross sections at 30 keV $\sigma_{n,\gamma}$ and test different "a" values against Γ_γ and $\sigma_{n,\gamma}$ calculations.

We considered all the information from MU-84. In particular, first from D_{OBS} for s-wave resonances and from the analysis of discrete level schemes, we determined the level density parameters a, U_x and T. These gave us the local trends for the respective systematics. Then we checked isotopic values

of a, U_x, T and local systematics by comparison of calculated $\Gamma_\gamma(B_n,J,\pi)$ for s- and p-wave resonances with the respective values from MU-84. Finally, we checked the entire parametrization by comparison of calculated and experimental total $\sigma_{n,\gamma}$ (E). As a result, we arrived at the systematics shown in Figs. 8 and 9 for a, U_x and T. As one can see, a-values are affected by a much larger spread than the corresponding T- and U_x- values. In particular, for higher masses, as shown in Fig. 9, a-values corresponding to e-e targets exhibit a distinct behavior according to different isotope families. The same cannot be clearly identified for the data corresponding to even-odd, odd-odd, odd-even targets for which overall systematics common to all families appear to be fully adequate in most cases.

According to the discussion outlined in Section B.2.1, in extrapolating "a" systematics off the stability valley, a wider uncertainty range had to be allowed for "a", especially for cases in which B_n was much lower than that of isotopes in the stability valley. Of course, information as to the reliability of "a" comes primarily from the related quantity T. In all cases, uncertainties on a-, U_x-, and T-values adopted were estimated from consideration on the spread of data around the respective systematics.

The parametrization adopted, is summarized in Table 1. In column 2 of Table 1, uncertain target ground state spin and parity assignments are given in brackets. In some cases, all probable assignments are quoted, the first of which being the one adopted. In Table 1, parameter uncertainties are also quoted.

In Figs. 12 and 13, comparison is made of the calculated total radiative widths for s- and p-wave resonances respectively with the systematics of MU-84. In some cases, especially for p-wave resonances, our calculated aver-

age radiative widths showed a strong spin dependence. Therefore, the calculated values given in Fig. 12 and 13 were obtained as weighted averages according to the statistical factor 2J+1. With that, we felt that we would obtain the best agreement with the average experimental values quoted in MU-84. One can see that, in general, Γ_γ^{calc} do not exhibit large deviations from the data typical of the stability valley. The only exceptions seem to be those compound nuclei characterized by very low neutron binding energies. In fact, a deviation of Γ_γ with respect to the systematics of the valley of stability can be expected when B_n is particularly low because the smaller B_n, the smaller the number of γ-transitions.

Preliminary neutron capture cross section results are given in Table 2 for a few energies in the range 1 keV $\leq E_n \leq$500 keV. Sensitivity calculations were performed for $^{135}_{56}Ba$ (n,γ) reaction cross section in the whole energy range and are shown in Table 3. These were obtained by letting target and compound nucleus parameters vary according to the respective uncertainties quantified in Table 1. The case considered is one associated with the largest uncertainty. In addition, the unknown ground state spin and parity values were allowed to vary from $7/2^-$ to $11/2^+$, while the unknown neutron inelastic competition threshold was allowed to vary in the range 0-60 keV, as shown in Table 1.

In Table 3, results of sensitivity and error calculations in $^{135}Ba(n,\gamma)$ are shown. Percent errors quoted were derived using error propagation theory. To this end, parameter uncertainties were used with the meaning of standard deviations. In doing error calculations "a" and U_x, as taken from the respective systematics, are to be considered as uncorrelated in spite of Eq. 23. Errors from uncertainties due to target parameters and due to com-

pound nucleus parameters are given separately as well as the total error due to error propagation of both target and compound nucleus parameters.

From the results of our detailed sensitivity and error calculations in ^{135}Ba (n,γ) one can conclude that:

- the total uncertainty from target parametrization is negligible below the threshold for neutron inelastic competition; whereas above, it becomes comparable to that due to the compound nucleus parametrization,
- uncertainty from ground state spin and parity assignments results in a maximum 30% in target parametrization uncertainty,
- uncertainty from target parametrization is dominated by the uncertainty in the threshold of neutron inelastic competition, followed by that in the level density parameters "a" and especially U_x,
- uncertainty from compound nucleus parametrization is dominated by the uncertainty in U_x followed by that in "a",
- total uncertainty increases with incident neutron energy because the number of open competing channels increases, each of which carrying its own uncertainty contribution.

Error calculations were also performed for at least one isotope of each family of interest; we chose the isotope with the highest fission yield. For a few isotope families, error calculations were performed for all isotopes. Results are presented in Table 2. Note that errors are asymmetric about the central value. At 1 keV, the percent negative standard deviation $\Delta\sigma_{n,\gamma}(-)$ ranges between 20% and 50% with a narrow peak around 35%, which includes 60% of all cases considered. $\Delta\sigma_{n,\gamma}(+)$ ranges from 30% to 110% with a wide

peak around 50%; 70% of all cases range between 40% and 70%. At 500 keV, $\Delta\sigma_{n,\gamma}(-)$ ranges from 30% to 110% with a peak around 50%, while 80% of cases range from 40% to 60%; $\Delta\sigma_{n,\gamma}(+)$ (exception made for ^{102}Nb) ranges from 30% to 200% with a peak around 80%, while 65% of all cases range from 60% to 90%. To summarize, we conclude from the present calculations that for ~70% of all cases, the standard deviation is less than a factor of 2.

Sensitivity calculations to OMP are not easy to do because of the difficulty of relating uncertainties from OMP to those of quantities calculated by the optical model. A way to get around this problem is to use a strength function model because strength functions are measured quantities which can be expressed in terms of the optical model. Accordingly, the branching ratio in Eq. 1 can be expressed as:

$$\langle\sigma_{n,\gamma}\rangle_{\ell} \alpha \frac{S_{\ell} \langle\Gamma_{\gamma}/D\rangle_{\ell}}{\langle\Gamma_{\gamma}/D\rangle_{\ell} + \sum_{\ell'} \ell'} W_{\ell\ell'} \qquad \text{(Eq. 28)}$$

As has already been indicated, one requirement to be imposed on the optical model parametrization is to fit strength functions. This implies that maximum uncertainties expected in $\sigma_{n,\gamma}$ in Eq. 1 from the optical model, do not exceed the maximum spread of strength functions around the systematics of Figs. 2 and 3 (as long as the neutron absorption is not affected too much by higher neutron excesses of the presently investigated isotopes). In particular, because $\langle\Gamma_{\gamma}/D\rangle_{\ell} \ll \sum_{\ell}, T_{\ell}$, a partial cancelation takes place between incoming and outgoing channels in the numerator and denominator of Eq. 28, which tends to neutralize strength functions and optical

model T_ℓ-uncertainties. Cancelation becomes complete when, as at low energies, in the denominator of Eq. 28, only one ℓ'-value dominates. Accordingly, we believe that compared to the major uncertainties (e.g., from the level density parametrization), uncertainties from optical model quantities can be neglected.

Uncertainties from the photon absorption cross section σ_γ, which cannot be guessed, come from the fact that when B_n is low, the low energy tail of the Lorentzian becomes more important where extrapolations are not very reliable. No significant uncertainties are expected from the extrapolation of gian resonance parameters as far as the value and sign of deformation parameters is known.

An equal distribution between the two parities was assumed because of a complete lack of adequate information to perform a parity distribution analysis. We did not study the effect of extreme hypotheses like $p(\pi=+)=1$ and $p(\pi=-)=1$ and did not include such results as an estimate of the uncertainty propagated in neutron capture due to the uncertainties in the parity distribution.

D. CONCLUSIONS

The results of our sensitivity calculations pinpoint those parameters which have the greatest effect upon the accuracy of our model calculations, namely level density parameters and nuclear structure data, which are responsible for over 80-90% of the final estimated uncertainty.

No sophisticated nuclear modeling has been performed to generate missing information such as energy, spin, and parity of discrete levels. In many cases, the spin and parity of the target ground state were unknown. These

have been estimated by use of the Nilsson model and by comparison with neighboring isotopes of similar nuclear even-odd characteristics. The same was done to estimate the energy of the first excited states in target nuclei, which, being the threshold of (n,n') competition, can be very important in the accuracy of the results. Revision of these input data following more sophisticated nuclear theory by experts in this area would permit a reduction in the estimated uncertainties where I^{π} are unknown as experimentally deduced values.

These results should be regarded as preliminary ones in that all parameters were taken by systematics for most nuclei. If lower uncertainties are important, then a second iteration should be done using the results of the sensitivity and error calculations to pinpoint those parameters requiring more reliable values for each case.

0612A-9/2/86

Acknowledgements

The authors greatly appreciate helpful comments and advise from Dr. R. White during the course of this work. The help of Mrs. Frances Scheffel of BNL in providing needed nuclear data is similarly appreciated. One of the authors wishes to thank Maureen and Don Gardner for helpful discussions.

This work was performed under the auspices of the U.S. Department of Energy by the Lawrence Livermore National Laboratory under contract number W-7405-ENG-48.

References

BE-74 V. Benzi, G. Reffo, M. Vaccari, "In the Calculation of Total Radiative Widths of Neutron Resonances," IAEA Report 169, Vol. III, page 123 (1974), proceedings of the meeting "Fission Product Nuclear Data," Bologna 26-30 Nov. 1983.

BE-84 R. Bengtsson, P. Moller, J. R. Nix, Jing-ye Zhang, Physica Scripta 29, 402 (1984).

FA-74 F. Fabbri, G. Reffo, CERBERO: A Fortran Programme for the Calculation of Nuclear Reaction Cross Sections, CNEN Report RT/F1(74)36, (1974).

FA-77 F. Fabbri, G. Fratamico, G.Reffo, CERBERO 2: Improved Version of the CERBERO Computer Code. CNEN Report RT/F1(77)6, (1977).

GI-65 A. Gilbert, A. G. W. Cameron, Can. Journ. of Phys. 43, 1446 (1965).

GR-77 H. Gruppelaar, G. Reffo, N.S.E. 62, 756, (1977).

LE-78 C. M. Lederer, V. Shirley, "Table of Isotopes," John Wiley and Sons (1978).

MO-81 P. Moller, J. R. Nix, "Atomic Data and Nuclear Data Tables," 26, 165 (1981).

MO-83 P. A. Moldauer, Nucl. Phys. 47, 65 (1983).

MU-84 S. F. Mughabghab, "Neutron Cross Sections," Vol. 1, Neutron Resonance Parameters and Thermal Cross Sections, Academic Press, Inc., (1984).

RO-68 N. Rosenszweig, Nucl. Phys. 118, 650 (1968).

RE-76 G. Reffo, F. Fabbri, H. Gruppelaar, N.C. Letters 17, 1 (1976).

RE-78 G. Reffo, F. Fabbri, N.S.E. 66, 251 (1978).

RF-78 G. Reffo, "Parameter Systematics for Statistical Theory Calculations of Neutron Reaction Cross Sections," ENEA Report RT/F1(78)11.

RE-83 G. Reffo, F. Fabbri, K. Wisshak, F. Kaeppeler, Nucl. Sci. Eng. 86, 168 (1983).

WA-77 A. H. Wapstra, K. Bos., The 1977 Atomic Mass Evaluation in Four Parts, At. Data Nucl. Data Tables, 19, 177 (1977).

WA-83 G. Walter, B. Leugers, F. Kaeppeler, Z. Y. Bao, D. Erbe, G. Rupp, G. Reffo, F. Fabbri, KFK Report 3652 (1983), and submitted to NSE 1985.

WI-82 K. Wisslak, F. Kaeppeler, G. Reffo, F. Fabbri, Nucl. Sci. Eng. 80m 630 (1982).

Tables

Figure Captions

Figure 1: Potential scattering radius R vs. mass number A, as calculated from Moldauer OMP compared to the systematic of Mughabghab, MU-84. Points with error bars represent experimentally deduced values as summarized in MU-84.

Figure 2: L=0 strength functions S_0 vs A, as calculated from Moldauer OMP compared to the systematics in MU-84. Points with error bars are experimentally deduced results as summarized in MU-84.

Figure 3: L=1 strength functions S_1 vs A, as calculated from Moldauer OMP compared to the systematics in MU-84. Points with error bars are experimentally deduced results as summarized in MU-84.

Figure 4: L=2 strength functions S_2 vs A, as calculated from Moldauer OMP compared to the systematics in MU-84. Points with error bars are experimentally deduced results as summarized in MU-84.

Figure 5: Shell model single particle state density g vs. neutron number N and proton number Z, for different deformation parameters β..

Figure 6: Overall systematics of the level density parameter a vs. neutron number. See RF-78 for details.

Figure 7: Overall systematics of matching energy U_x and of nuclear temperature T vs. neutron number. Origin of points is discussed in the text. Circled dots refer to Sn isotopes.

Figure 8: Local systematics of level density parameters a, T, and U_x vs. neutron number around the magic number N=50.

Figure 9: Local systematics of level density parameters vs. neutron number N around the magic number N=82.

Figure 10: Giant resonance parameter systematics for spherical nuclei vs. mass number A.

Figure 11: Giant resonance parameter systematics vs. deformation parameter β and vs. mass number A after ref. RF-78.

Figure 12: Calculated s-wave radiative widths compared to the systematics of ref. 2 vs. mass number A.

Figure 13: Calculated p-wave radiative widths compared to the systematics of ref. 2 vs. mass number A.

TABLE 1: Parameters Used in Calculations Summarized in Table 2.
The parameters are discussed in the text. The superscript 'T' indicates target isotopes.

Isotope	I^{π} Ground State Spin and Parity	E_1 MeV EXPTL	E_1 MeV Guessed	E_{cut} MeV	a MeV^{-1}	U_x MeV	σ^2LVL EXPTL	σ^2LVL Guessed	β_2 BE-84
34 Se 87^T	$5/2^+7/2^+$	- -	0.20±0.10	0.20±0.10	13.8±2	6.0+1	- -	7±5	- -
34 Se 88^T	0^+	- -	0.50±0.10	0.50±0.10	14.0±2	6.5±1	- -	5±3	0.18
34 Se 89	$5/2^+7/2^+$	- -	0.15±0.10	0.15±0.10	15.7±2	6.7±1	- -	7±5	0.18
35 Br 87^T	$(3/2^-)$	- -	0.35±0.10	0.35±0.10	11.8±2	5.5±1	- -	7±5	- -
35 Br 88^T	(1^-)	- -	0.20±0.15	0.20±0.15	12.8±2	6.0±1	- -	7±5	0.15
35 Br 89^T	$3/2^-1/2^-5/2^-$	- -	0.30±0.10	0.30±0.10	13.9±2	6.4±1	- -	7±5	0.15
35 Br 90	- -	- -	- -	0.00±0.00	14.8±2	6.5±1	- -	7±5	0.18
36 Kr 89^T	$5/2^+7/2^+$	- -	0.40±0.10	0.40±0.10	13.8±2	6.0±1	- -	7±5	- -
36 KR 90^T	0^+	0.708	- -	1.00	13.9±2	6.4±1	- -	5±2	0.15
36 Kr 91^T	$5/2^+7/2^+$	- -	0.40±0.10	0.40±0.10	15.7±2	6.5±1	- -	7±5	0.17
36 Kr 92	0^+	- -	- -	1.20	15.7±2	6.6±1	- -	5±3	0.17
37 Rb 91^T	$7/2^+9/2^+5/2^+$	0.108	- -	0.108	14.0±2	6.4±1	- -	7±5	- -
37 Rb 92^T	(1^-)	0.143	- -	0.143	14.8±2	6.5±1	- -	7±5	0.20
37 Rb 93^T	$5/2^+$	0.254	- -	0.350	15.7±2	6.5±1	- -	7±5	0.20
37 Rb 94^T	3^-	0.191	- -	0.191	16.3±2	6.5±1	- -	7±5	0.25
37 Rb 95	$5/2^+$	- -	0.10±0.07	0.10±0.07	16.8±2	6.5±1	- -	7±5	0.27
38 Sr 92^T	0^+	0.816	- -	1.000	14.0±2	6.4±1	- -	5±3	- -
38 Sr 93^T	$7/2^+$	0.214	- -	0.214	15.7±2	6.5±1	6.25	7±3	0.15
38 Sr 94^T	0^+	0.837	- -	2.614	15.7±2	6.3	3.4	- -	0.20
38 Sr 95^T	$7/2^+5/2^+11/2^-$	0.203	- -	0.203	17.1±2	6.6±1	5.6	- -	0.25
38 Sr 96^T	0^+	0.815	- -	1.900	16.8±2	6.6±1	1.9	- -	0.30
38 Sr 97^T	$7/2^+5/2^-9/2^+11/2^-$	- -	0.10±0.05	0.10±0.05	18.2±2	6.5±1	- -	7±5	0.30
38 Sr 98	0^+	0.144	- -	0.144	17.6±2	6.5±1	4.22	- -	0.32

Isotope	I^{π} Ground State Spin and Parity	E_1 MeV EXPTL	E_1 MeV Guessed	E_{cut} MeV	a MeV^{-1}	U_x MeV	σ^2LVL EXPTL	σ^2LVL Guessed	β_2 BE-84
39 Y 95[T]	$1/2^-$	0.689	- -	0.700	15.6±2	6.6±1	- -	7±5	- -
39 Y 96[T]	0^-	0.101	- -	0.15	16.3±2	6.6±1	1.8	- -	0.30
39 Y 97[T]	$1/2^-$	0.668	- -	0.668	16.8±2	6.6±1	- -	7±5	0.30
39 Y 98	1^+	0.12	- -	0.17	17.3±2	6.5±1	- -	7±5	0.30
39 Y 99[T]	$1/2^-$	- -	0.1±0.07	0.1±0.07	17.6±2	6.4±1	- -	7±5	0.32
39 Y 100	- -	- -	0.0	0.0	17.8±2	6.4±1	- -	7±5	0.32
40 Zr 98[T]	0^+	0.855	- -	0.900	16.8±2	6.6±1	- -	5±3	- -
40 Zr 99[T]	$1/2^+$	0.122	- -	0.300	18.0±2	6.6±1	3.5	- -	0.30
40 Zr 100[T]	0^+	0.213	- -	0.300	17.6±2	6.6±1	8.6	- -	0.30
40 Zr 101[T]	$7/2^+11/2^-5/2^+9/2^+$	- -	0.1±0.07	0.1±0.07	18.5±2	6.6±1	- -	7±5	0.32
40 Zr 102[T]	0^+	0.153	- -	0.2	17.9±2	6.6±1	- -	5±3	0.32
40 Zr 103[T]	$7/2^+5/2^+11/2^-$	- -	0.1±0.07	0.1±0.07	18.5±2	6.5±1	- -	7±5	0.32
40 Zr 104	0^+	- -	0.0	0.0	17.5±2	6.5±1	- -	5±3	0.33
41 Nb 101[T]	$9/2^+7/2^+5/2^+$	- -	0.1±0.07	0.1±0.07	18.1±2	6.6±1	- -	7±5	- -
41 Nb 102[T]	(1^+)	- -	0.1±0.07	0.1±0.07	18.3±2	6.6±1	- -	7±5	0.30
41 Nb 103	$5/2^+$	0.127	- -	0.4	18.3±2	6.6±1	- -	7±5	0.30
41 Nb 104[T]	(1^+)	- -	0.1±0.07	0.1±0.07	18.2±2	6.6±1	- -	7±5	0.30
41 Nb 105	$5/2^+5/2^-9/2^+1/2^-$	- -	0.1±0.07	0.1±0.07	18.0±2	6.6±1	- -	7±5	0.30
42 Mo 102[T]	0^+	0.297	- -	0.35	17.6±2	6.6±1	- -	5±1	- -
42 Mo 103[T]	$3/2^+$	0.103	- -	0.3	18.5±2	6.6±1	- -	9±2	0.27
42 Mo 104[T]	0^+	0.193	- -	0.25	17.8±2	6.6±1	- -	6±3	0.27
42 Mo 105[T]	$7/2^+5/2^+11/2^-$	0.095	- -	0.15	18.5±2	6.5±1	- -	7±5	0.27
42 Mo 106	0^+	0.172	- -	0.2	17.5±2	6.5±1	- -	5±3	0.27
43 Tc 106[T]	(3^+)	- -	0.1±0.07	0.1±0.07	18.4±2	6.5±1	- -	7±5	- -
43 Tc 107[T]	$7/2^+9/2^+5/2^-1/2^-$	- -	0.1±0.07	0.1±0.07	18.2±2	6.4±1	- -	7±5	0.25
43 Tc 108	(3^+)	- -	0.1±0.07	0.1±0.07	17.9±2	6.3±1	- -	7±5	0.25

Page 3 Isotope	I^{π} Ground State Spin and Parity	E_1 MeV EXPTL	E_1 MeV Guessed	E_{cut} MeV	a MeV^{-1}	U_x MeV	σ^2LVL EXPTL	σ^2LVL Guessed	β_2 BE-84
44 Ru 108[T]	0^+	0.243	- -	0.3	17.5±2	6.4±1	- -	5±3	- -
44 Ru 109	$7/2^+5/2^+11/2^-$	0.099	- -	0.15	18.1±2	6.3±1	- -	7±5	0.25
49 In 124[T]	2^+	0.037	- -	0.1	16.7±2	4.6±1	- -	7±5	- -
49 In 125	$9/2^+$	0.181	- -	0.2	16.6±2	4.5±1	- -	7±5	0.05
50 Sn 130[T]	0^+	1.220	- -	2.0	14.5±2	4.0±1	- -	5±3	- -
50 Sn 131[T]	$3/2^+$	0.335	- -	0.4	13.8±2	3.6±1	- -	5±3	-0.05
50 Sn 132	0^+	4.035	- -	4.5	12.7±2	2.6±0.5	- -	5±3	-0.05
51 Sb 130[T]	4^+5^+	0.070	- -	0.07	15.9±2	4.3±1	- -	5±3	- -
51 Sb 131[T]	$7/2^+$	- -	0.2±0.10	0.2±0.1	15.3±2	4.0±1	- -	7±3	-0.05
51 Sb 132[T]	4^+	0.085	- -	0.085	14.4±2	3.6±1	- -	5±3	-0.05
51 Sb 133[T]	$7/2^+$	0.963	- -	0.963	13.4±2	2.6±1	- -	7±3	-0.05
51 Sb 134	(0^-)	- -	0.1±0.07	0.1±0.07	15.8±2	3.3±1	- -	5±3	-0.05
52 Te 130[T]	0^+	0.84	- -	0.84	16.5±2	4.4±1	- -	7±5	- -
52 Te 131[T]	$3/2^+$	0.64	- -	0.64	18.0±2	4.3±1	2.25	- -	0.05
52 Te 132[T]	0^+	1.85	- -	1.85	15.0±2	4.3±1	13.0	- -	-0.05
52 Te 133[T]	$3/2^+$	- -	0.45±0.2	0.45±0.2	16.1±2	3.6±1	- -	10±5	-0.05
52 Te 134	0^+	1.90	- -	1.90	16.0±2	3.0±1	11	- -	-0.05
52 Te 135[T]	$7/2^-$	- -	0.45±0.2	0.45±0.2	16.3±2	3.3±1	- -	10±5	-0.05
52 Te 136	0^+	- -	0.9±0.2	0.90±0.2	17.8±3	3.7±1	- -	10±5	-0.05
53 I 132[T]	4^+	0.022	- -	0.2	16.0±2	4.3±1	- -	10±2	- -
53 I 133[T]	$7/2^+$	0.312	- -	0.4	15.3±2	4.1±1	- -	10±2	0.05
53 I 134[T]	(4^+)	0.044	- -	0.3	14.5±2	3.5±1	8	- -	0.05
53 I 135[T]	$7/2^+$	- -	0.95±0.3	0.95±0.3	13.6±2	2.5±1	- -	8±5	0.05
53 I 136[T]	2^-	0.080	- -	0.08	15.6±2	3.3±1	4	- -	0.05
53 I 137[T]	$7/2^+$	0.243	- -	0.243	17.5±2	4.0±1	- -	6±3	0.05
53 I 138[T]	2^-	0.06±0.03		0.06±0.03	19.4±2	4.6±1	- -	6±3	0.05
53 I 139	- -	- -	0.05±0.05	0.05±0.05	26.2±2	5.0±1	- -	6±3	0.08

Page 4 Isotope	I^{π} Ground State Spin and Parity	E_1 MeV EXPTL	E_1 MeV Guessed	E_{cut} MeV	a MeV^{-1}	U_x MeV	σ^2LVL EXPTL	σ^2LVL Guessed	β_2 BE-84
54 Xe 135^T	$3/2^+$	0.288	- -	0.60	13.6±2	3.6±1	- -	7±5	- -
54 Xe 136^T	0^+	2.400	- -	2.40	11.0±2	3.5±1	- -	5±2	0.05
54 Xe 137^T	$7/2^-$	1.500	- -	1.50	14.0±2	3.8±1	4.5	- -	0.05
54 Xe 138^T	0^+	0.590	- -	0.59	15.1±2	3.8±1	3.2	- -	0.05
54 Xe 139^T	$7/2^-$	0.500	- -	0.50	18.0±2	4.5±1	- -	5±3	0.08
54 Xe 140^T	0^+	0.370	- -	0.37	18.7±2	4.8±1	- -	5±3	0.10
54 Xe 141	- -	- -	0.15±0.15	0.15±0.15	21.7±2	5.0±1	- -	5±3	0.10
55 Cs 139^T	$7/2^+$	0.218	- -	0.218	14.0±2	3.0±1	- -	5±3	- -
55 $Cs140^T$	(2-)	0.148	- -	0.148	18.0±2	4.9±1	2.3	- -	0.10
55 Cs 141^T	$7/2^+$	0.068	- -	0.068	19.9±2	5.2±1	- -	5±3	0.15
55 Cs 142^T	(2-)	0.011	- -	0.110	21.7±2	4.9±1	- -	5±3	0.15
55 Cs 143^T	$(7/2^+)$	0.030	- -	0.030	23.2±2	5.5±1	- -	5±3	0.17
55 Cs 144	- -	- -	0.0	0.0	24.6±2	5.4±1	- -	3±2	0.17
56 Ba 141^T	$(7/2^-)$	0.6±0.3	- -	0.6±0.3	20.3±2	4.5±1	- -	5±2	- -
56 Ba 142^T	0^+	1.5	- -	1.5	21.7±2	5.4±1	3.40	- -	0.12
56 Ba 143^+	$(7/2^-)$	0.03	- -	0.03	24.0±2	5.7±1	- -	5±2	0.12
56 Ba 144^T	0^+	0.75	- -	0.75	24.8±2	5.4±1	- -	5±1	0.15
56 Ba 145^T	$9/2^-13/2^+7/2^-$	- -	0.03±0.03	0.03±0.03	26.4±2	5.4±1	- -	5±2	0.15
56 Ba 146^T	0^+	1.11	- -	1.11	26.3±2	5.4±1	4.15	- -	0.18
56 Ba 147	$7/2^-9/2^-13/2^+$	- -	0.03±0.03	0.03±0.03	26.1±2	5.5±1	- -	5±3	0.20
57 La 144^T	(2^-)	0.100	- -	0.1	23.00±2	4.7±1	- -	7±3	- -
57 La 145^T	$(7/2^+)$	0.065	- -	0.065	24.2±2	5.3±1	- -	7±3	0.17
57 La 146	(2^-)	0.120	- -	0.12	25.5±2	5.0±1	- -	9±3	0.17

TABLE 2: CALCULATED (n,γ) CAPTURE CROSS SECTIONS

TARGET	B_n(MeV)	E_n(keV): 1	30	100	300	500
Se-87*	5.538	90+70 -50	5.2+5 -3	2.3+2 -1	1.0+1.5 -1.0	0.5+0.8 -0.5
Se-88*	2.761	10+8 -5	0.7+0.6 -0.3	0.5+0.4 -0.2	0.3+0.3 -0.2	0.3+0.4 -0.2
Br-87	4.951	280+190 -125	21+12 -12	9.3+8 -5	6.2+5.7 -3.5	3.4+6.8 -4.0
Br-88*	3.751	34+28 -20	19+16 -10	1.0+1.3 -0.8	0.2+1.0 -0.6	0.07+0.2 -0.1
Br-89*	3.371	93+75 -50	5.4+5 -3	2.3+2.3 -1.5	1.8+2.4 -1.5	0.60+1.4 -0.8
Kr-89	6.461	280+190 -125	20+17 -11	8.6+7 -4	5.0+4 -2	3.2+5 -3
Kr-90	4.661	150+100 -70	12+10 -7	6.9+5 -3	6.1+5 -3	6+5 -3
Kr-91	5.451	135+100 -70	8+7 -4	3.4+3 -2	2+2 -1	1+2.6 -1.5
Rb-91	5.221	820+530 -350	80+74 -50	32+30 -20	12+12 -7	6+7 -4
Rb-92	5.871	520+320 -210	50+40 -30	21+17 -11	3.0+3.5 -2.0	1.0+1.3 -0.8
Rb-93	4.611	680+430 -280	62+60 -40	25+23 -14	13+12 -7	5.2+5.9 -3.5
Rb-94	5.161	620+390 -260	52+50 -30	21+19 -12	5+5 -3	1.0+1.4 -0.8
Sr-92	5.659	320	33	16	15	15
Sr-93	6.751	400	31	13	4.8	2
Sr-94	4.251	150	11	6.5	6	6

*Binding energy from Mo-81.

TABLE 2: CALCULATED (n,γ) CAPTURE CROSS SECTIONS--continued

TARGET	B_n(MeV)	E_n(keV): 1	30	100	300	500
Sr-95	6.001	380+290 -190	29+30 -20	12+14 -9	4.5+7 -4	1.8+3.5 -2.0
Sr-96	4.001	150	11	6.3	6	6
Sr-97	6.371	600	53	21	4.6	2
Y-95	5.268	1130+630 -420	170+140 -90	70+60 -40	49+36 -20	51+40 -24
Y-96	5.921	790	120	54	3.3	1.10
Y-97	4.981	890	120	52	39	43
Y-99	4.211	500	51	22	4.8	2.2
Zr-98	4.669	350	34	16	15	16.
Zr-99	6.781	570	69	29	4.6	1.9
Zr-100	4.521	280	26	13	3.8	1.9
Zr-101	6.901	1025+540 -360	130+110 -70	50+60 -40	11+20 -12	4.6+8 -5
Zr-102	4.081	177	14	8	14	0.8
Zr-103	6.111	400	37	17	2.7	1.1
Nb-101	5.481	1900	380	170	53	30
Nb-102	7.121	1950+630 -400	480+320 -200	220+400 -160	18+60 -18	5.8+11 -5.8
Nb-103	4.592	1030	130	54	13	5.4
Nb-104*	6.351	1290	230	100	7	2.3

TABLE 2: CALCULATED (n,γ) CAPTURE CROSS SECTIONS--continued

TARGET	B_n(MeV)	E_n(keV): 1	30	100	300	500
Mo-102	5.119	440	52	24	23	12
Mo-103	7.961	1550	310	130	31	14
Mo-104	4.711	300+190 -125	28+30 -18	14+12 -8	4.5+4.0 -3.0	2.5+2.5 -1.5
Mo-105*	6.901	900	111	44	10	4.6
Tc-106	7.551	2340	840	440	50	16
Tc-107*	4.072	550+300 -200	50+45 -30	21+25 -16	4.6+10 -4	2.1+3.5 -2.0
Ru-108	5.061	350+200 -130	38+35 -23	19+15 -9	8+7 -4	4+4 -2
In-124	7.471	2110+900 -600	310+200 -100	110+80 -50	27+30 -18	13+17 -10
Sn-130	5.171	90+36 -24	10+5 -3	5+3 -2	4+2 -1	4+2 -1
Sn-131	6.981	110	8.7	3.9	2.6	2.2
Sb-130	7.791	4197	556	276	114	67
Sb-131	5.581	710+400 -300	70+50 -30	32+23 -14	17+17 -10	11+13 -7
Sb-132	7.441	1500	170	77	34	22
Sb-133	2.961	22	1.3	0.6	0.34	0.32
Te-130	5.924	490	76	44	34	36
Te-131	8.083	1383	164	80	47	35

TABLE 2: CALCULATED (n,γ) CAPTURE CROSS SECTIONS--continued

TARGET	B_n(MeV)	E_n(keV): 1	30	100	300	500
Te-132	5.788	200+100 -60	28+15 -10	17+9 -6	13+7 -4	14+8 -5
Te-133	7.811	1000	113	57	37	30
Te-135	5.301	100	7.5	3.2	2	1.8
I-132		6500	800	320	144	89
I-133	6.14	1400+1100 -640	150+120 -70	70+62 -33	43+43 -20	30+30 -15
I-134	7.9	2700+2500 -1400	300+300 -150	100+120 -54	38+52 -21	27+40 -17
I-135	3.7	84+47 -31	5.8+4 -2	2.4+1.5 -1.1	1.4+1.2 -0.6	1.4+1.0 -0.6
I-136	5.361	510+250 -159	48+30 -19	22+15 -8	7+5.6 -2.8	3.8+3.0 -1.7
I-137	3.081	113.0+60 -40	8.4+5 -3	3.6+2.4 -1.5	2.0+1.7 -0.8	1.3+1.0 -0.6
I-138	4.471	422+250 -150	40+27 -16	11+9 -5	1.5+1.2 -0.6	0.7+0.6 -0.3
Xe-135	7.99	330	43	19	11	9.2
Xe-136	3.861	18+6 -4	2.4+0.5 -0.3	1.3+0.3 -0.2	0.9+0.3 -0.2	1.0+0.3 -0.2
Xe-137	5.886	170+80 -50	13+7 -5	5.5+3 -2	3.1+2.0 -1.3	2.8+2.0 -1.2
Xe-138	3.791	50+24 -17	5.3+3 -2	2.7+2 -1	2.1+1.4 -0.8	2.3+1.5 -0.9
Xe-139	5.501	190+90 -60	19+12 -7	10+7 -4	6.6+4.3 -2.5	7+4 -3
Xe-140	3.891	110+80 -50	16+11 -7	9+8 -4	6.7+5.1 -3.0	6+4 -3

TABLE 2: CALCULATED (n,γ) CAPTURE CROSS SECTIONS--continued

TARGET	B_n(MeV)	E_n(keV): 1	30	100	300	500
Cs-139	4.681	990+630 -390	93+60 -40	45+30 -20	25+21 -11	21+17 -10
Cs-140	5.831	1700+940 -620	130+70 -50	35+26 -15	6.7+5.5 -3.1	4+3 -2
Cs-141	4.021	970+550 -360	93+52 -35	41+26 -17	12+9 -5	7+5 -3
Cs-142	5.481	3200+1700 -1100	220+130 -80	40+29 -17	7.4+5.6 -3.2	4+3 -2
Cs-143	3.641	1300+900 -500	130+80 -50	40+29 -17	9+7 -4	5+4 -2
Ba-141	5.91	600+360 -210	54+36 -21	25+18 -10	15+10 -6	14+9 -5
Ba-142	4.26	210+160 -90	32+24 -15	20+16 -10	14+12 -7	5.4+5 -3
Ba-143	6.09	1300+900 -500	120+80 -50	45+36 -20	14+12 -6	8+7 -4
Ba-144	3.86	150+130 -70	23+19 -12	13+14 -7	3+4 -2	2.6+3.0 -1.4
Ba-145	5.81	910+873 -491	85+80 -48	35+43 -26	12+18.6 -9	7.5+9.8 -6.2
Ba-146	2.672	26+26 -14	3.5+4.0 -2.0	1.6+2.0 -1.0	0.3+0.4 -0.2	0.3+0.4 -0.2
La-144	6.061	7100+3100 -2400	620+270 -200	340+160 -120	32+26 -14	14+12 -7
La-145	4.611	5700+2700 -2000	490+220 -160	230+120 -90	60+44 -26	31+25 -14

TABLE 3: Sensitivity Calculations for $^{145}_{56}Ba$

Results from Standard Parameter and their Variations

Cross Sections (mb) / Nuclear Structure Data Variations	σ(1 keV)	σ(30 keV)	σ(100 keV)	σ(300 keV)	σ(500 keV)
Standard Parameters	910.0	85.0	35.0	12.0	7.6
Target Nucleus Nuclear Structure Data Variation					
$a + \Delta a$	910.0	85.0	34.0	11.0	6.2
$a - \Delta a$	910.0	85.0	37.0	14.0	9.2
$U_x + \Delta U_x$	910.0	85.0	28.0	7.0	3.7
$U_x - \Delta U_x$	910.0	85.0	41.0	18.0	13.0
$\sigma^2 + \Delta\sigma^2$	910.0	85.0	34.0	11.0	6.2
$\sigma^2 - \Delta\sigma^2$	910.0	85.0	39.0	16.0	11.0
I^{π}min.	998.0	93.0	35.0	10.0	5.7
I^{π}max.	671.0	65.0	30.0	14.0	10.0
$E_{cut} + \Delta E_{cut}$	910.0	86.0	40.0	14.0	8.0
$E_{cut} - \Delta E_{cut}$	910.0	82.0	32.0	11.6	7.1
Total percent error due to uncertainty in compound nucleus parameterization	+10 -26	+9 -24	+26 -26	+67 -47	+107 -60
Compound Nucleus Nuclear Structure Data Variation					
$a + \Delta a$	1324.0	125.0	53.0	20.0	12.0
$a - \Delta a$	623.0	61.0	23.0	7.8	4.6
$U_x + \Delta U_x$	1665.0	154.0	66.0	24.0	14.0
$U_x - \Delta U_x$	501.0	50.0	19.0	6.6	4.0
$\sigma^2 + \Delta\sigma^2$	920.0	87.0	35.0	13.0	7.5
$\sigma^2 - \Delta\sigma^2$	899.0	86.0	36.0	12.0	7.4
$\beta + \Delta\beta$	979.0	91.0	37.0	13.0	7.9
$\beta - \Delta\beta$	896.0	83.0	34.0	12.0	7.4
Total percent error due to uncertainty in compound nucleus parameterization	+95 -55	+94 -50	+100 -57	+120 -57	+100 -62
Total percent error	+96 -61	+94 -55	+103 -79	+137 -74	+146 -86

1021A

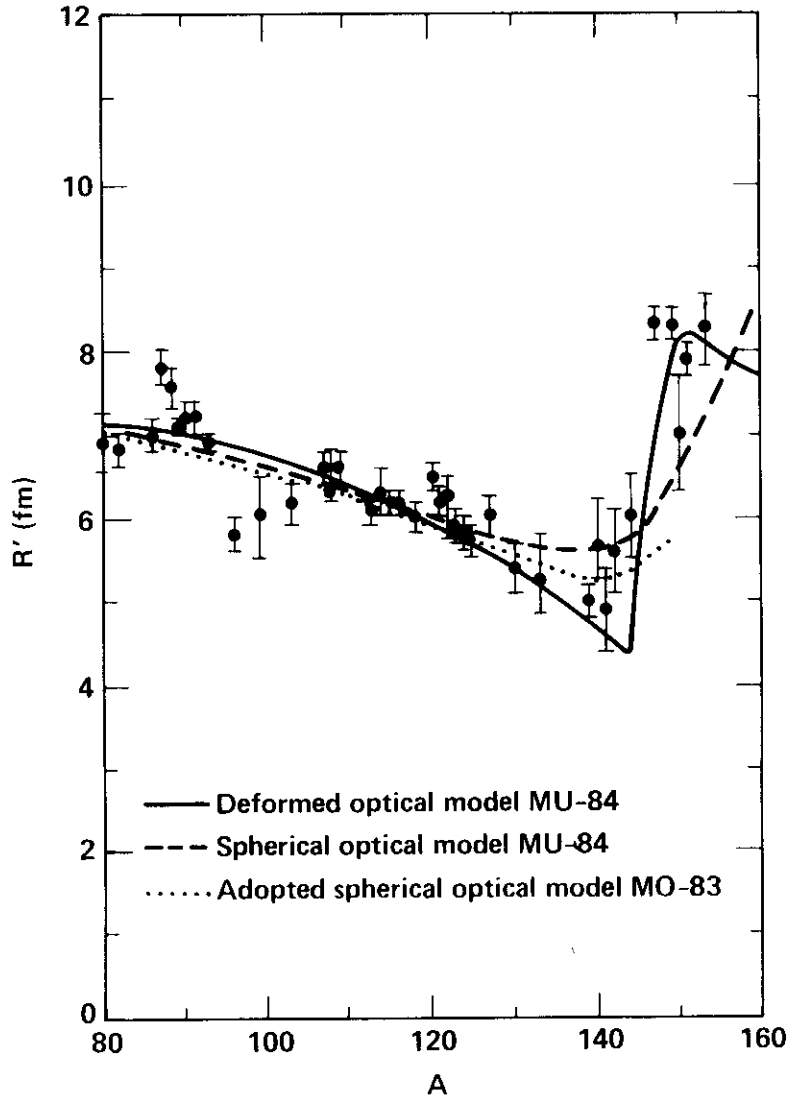
12
10
8
6
4
2
0
R' (fm)
80
100
120
140
160
A
Deformed optical model MU-84
Spherical optical model MU-84
Adopted spherical optical model MO-83

Figure 1

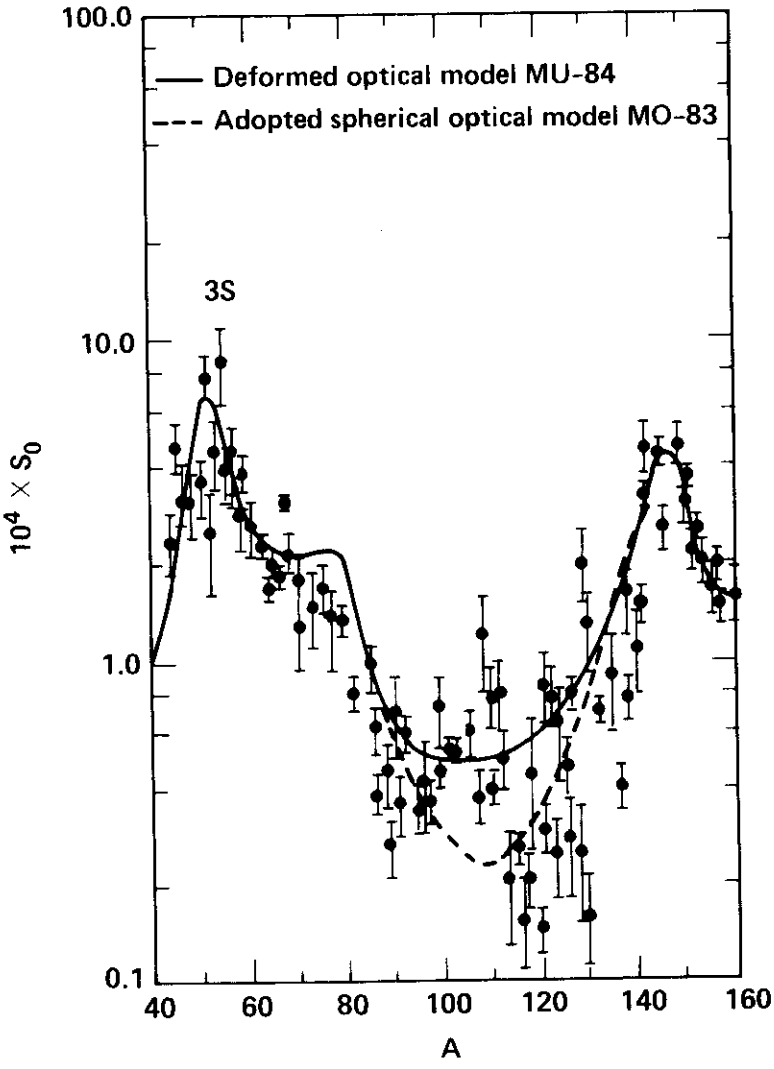
100.0
10.0
1.0
0.1
$10^4 \times S_0$
Deformed optical model MU-84
Adopted spherical optical model MO-83
3S
40
60
80
100
120
140
160
A

Figure 2

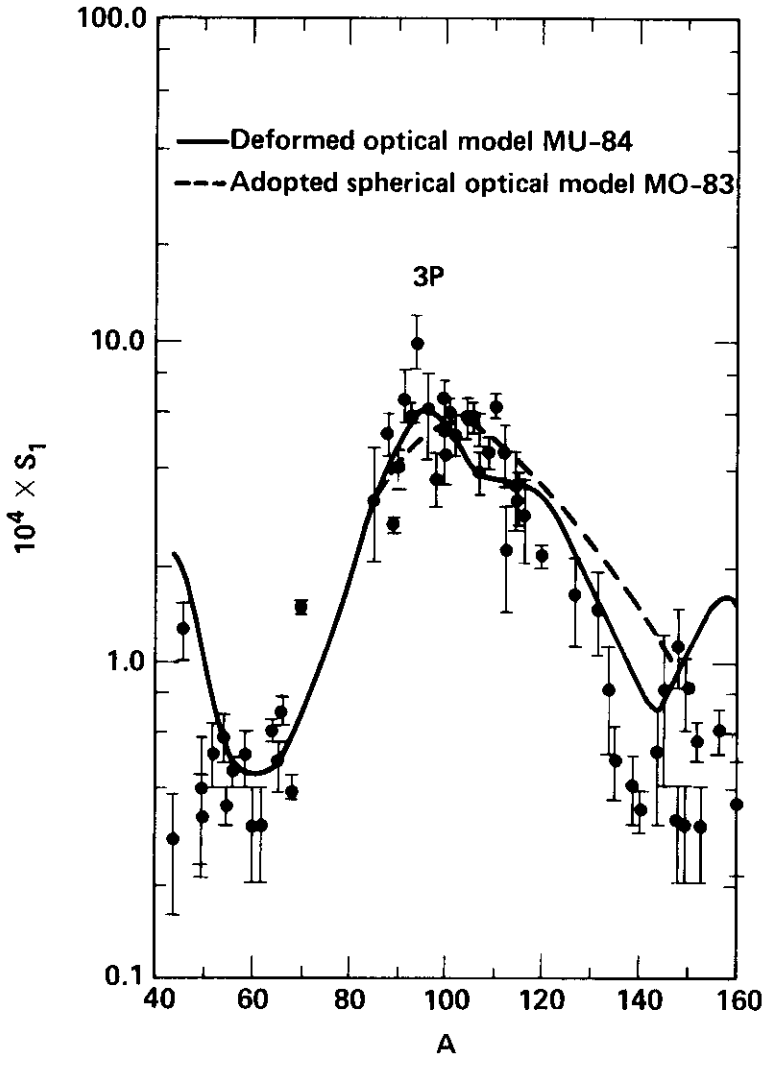
100.0
10.0
1.0
0.1
40
60
80
100
120
140
160
A
$10^4 \times S_1$
—Deformed optical model MU-84
---Adopted spherical optical model MO-83
3P

Figure 3

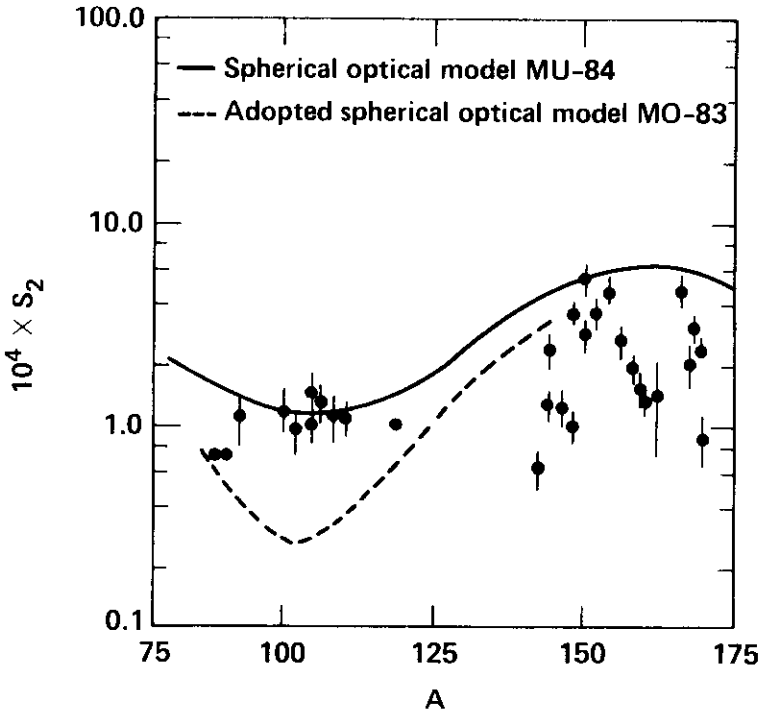
100.0
10.0
1.0
0.1
$10^4 \times S_2$
Spherical optical model MU-84
Adopted spherical optical model MO-83
75
100
125
150
175
A

Figure 4

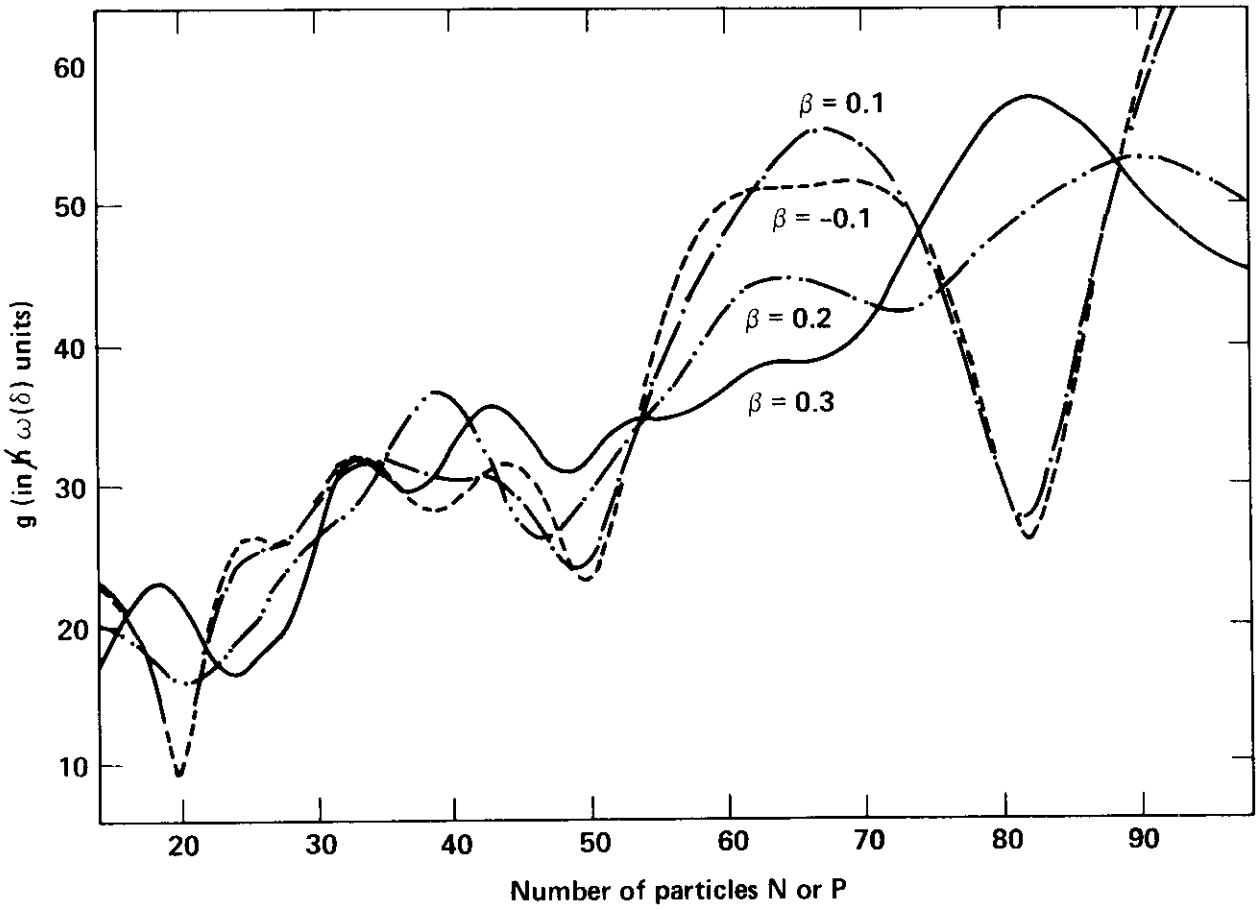
60
50
40
30
20
10
g (in $\hbar\omega(\delta)$ units)
β = 0.1
β = -0.1
β = 0.2
β = 0.3
20
30
40
50
60
70
80
90
Number of particles N or P

Figure 5

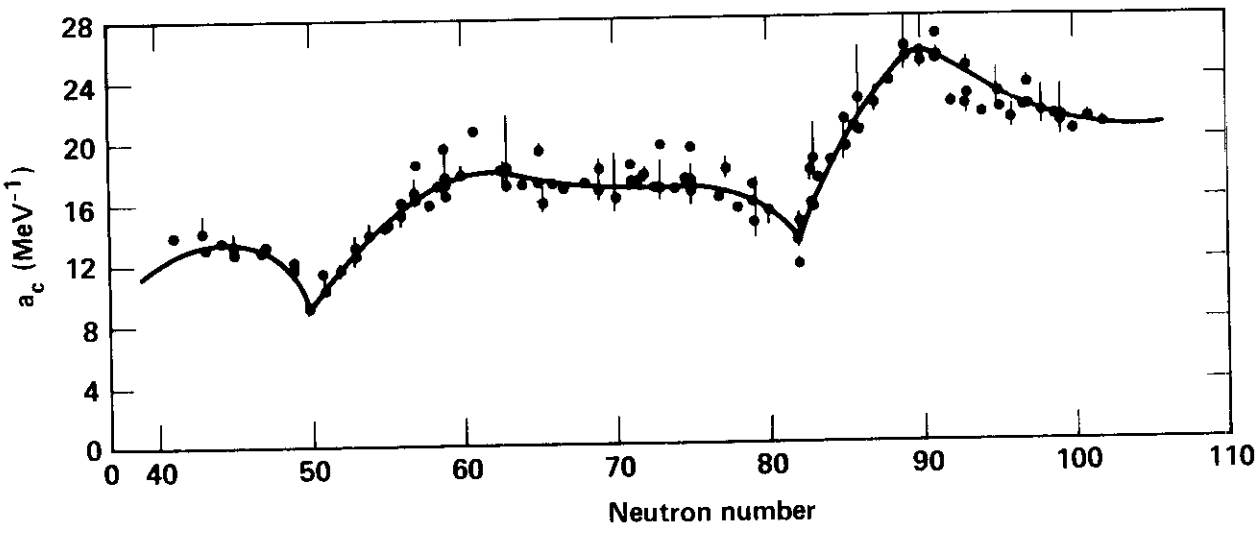
28
24
20
16
12
8
4
0
a_c (MeV^{-1})
0
40
50
60
70
80
90
100
110
Neutron number

Figure 6

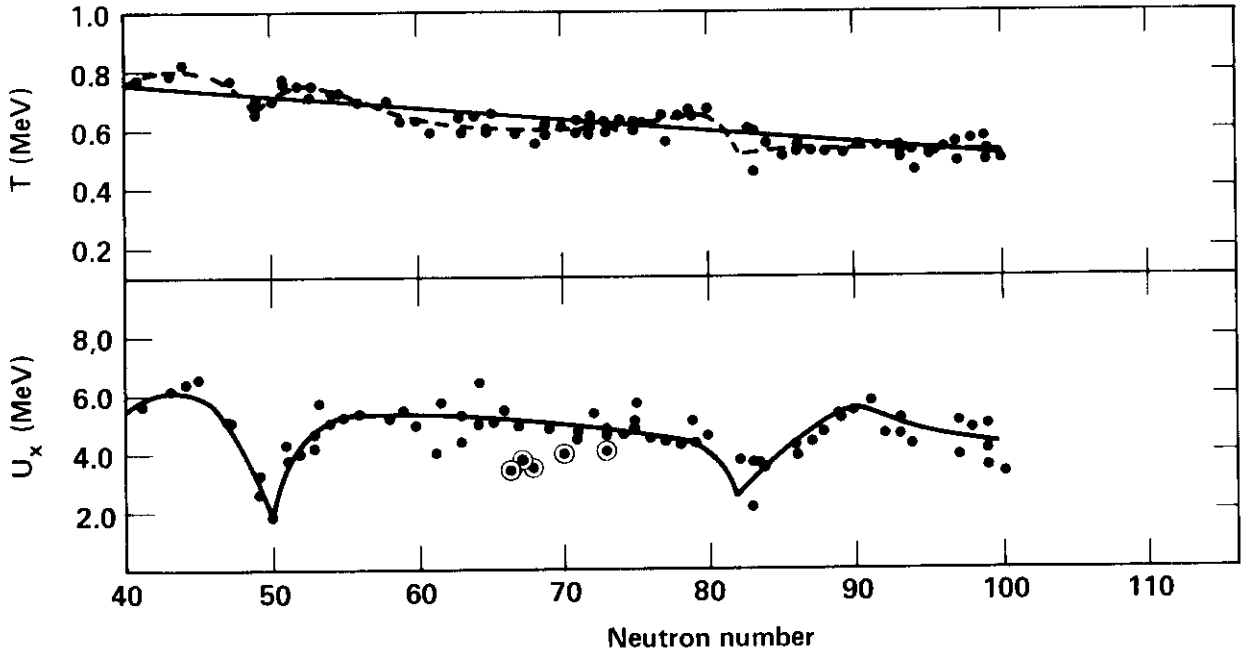
1.0
0.8
0.6
0.4
0.2
T (MeV)
8,0
6.0
4.0
2.0
U_x (MeV)
40
50
60
70
80
90
100
110
Neutron number

Figure 7

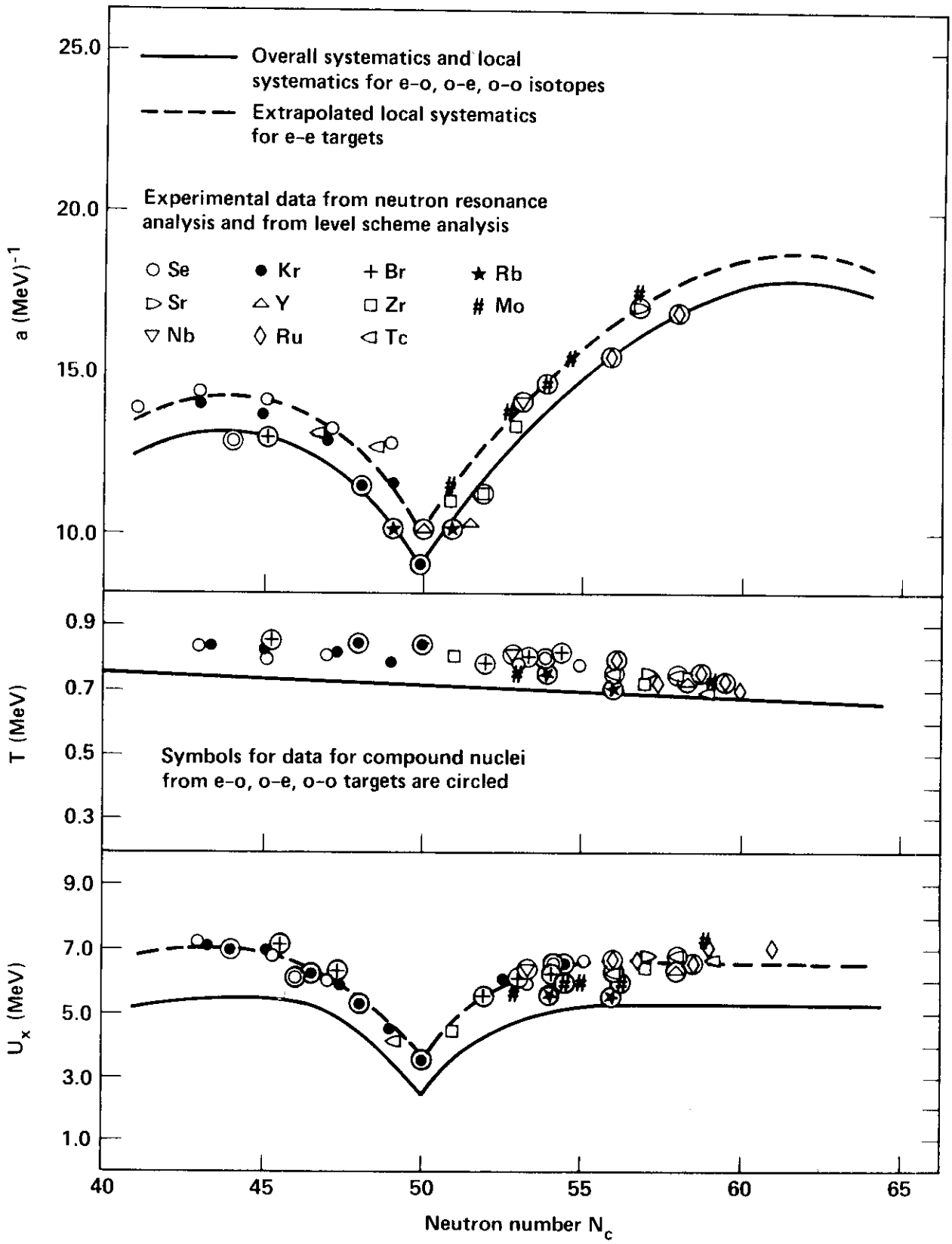
Overall systematics and local systematics for e-o, o-e, o-o isotopes
Extrapolated local systematics for e-e targets
Experimental data from neutron resonance analysis and from level scheme analysis
Se
Kr
Br
Rb
Sr
Y
Zr
Mo
Nb
Ru
Tc
a (MeV)$^{-1}$
25.0
20.0
15.0
10.0
T (MeV)
0.9
0.7
0.5
0.3
Symbols for data for compound nuclei from e-o, o-e, o-o targets are circled
U_x (MeV)
9.0
7.0
5.0
3.0
1.0
40
45
50
55
60
65
Neutron number N_c

Figure 8

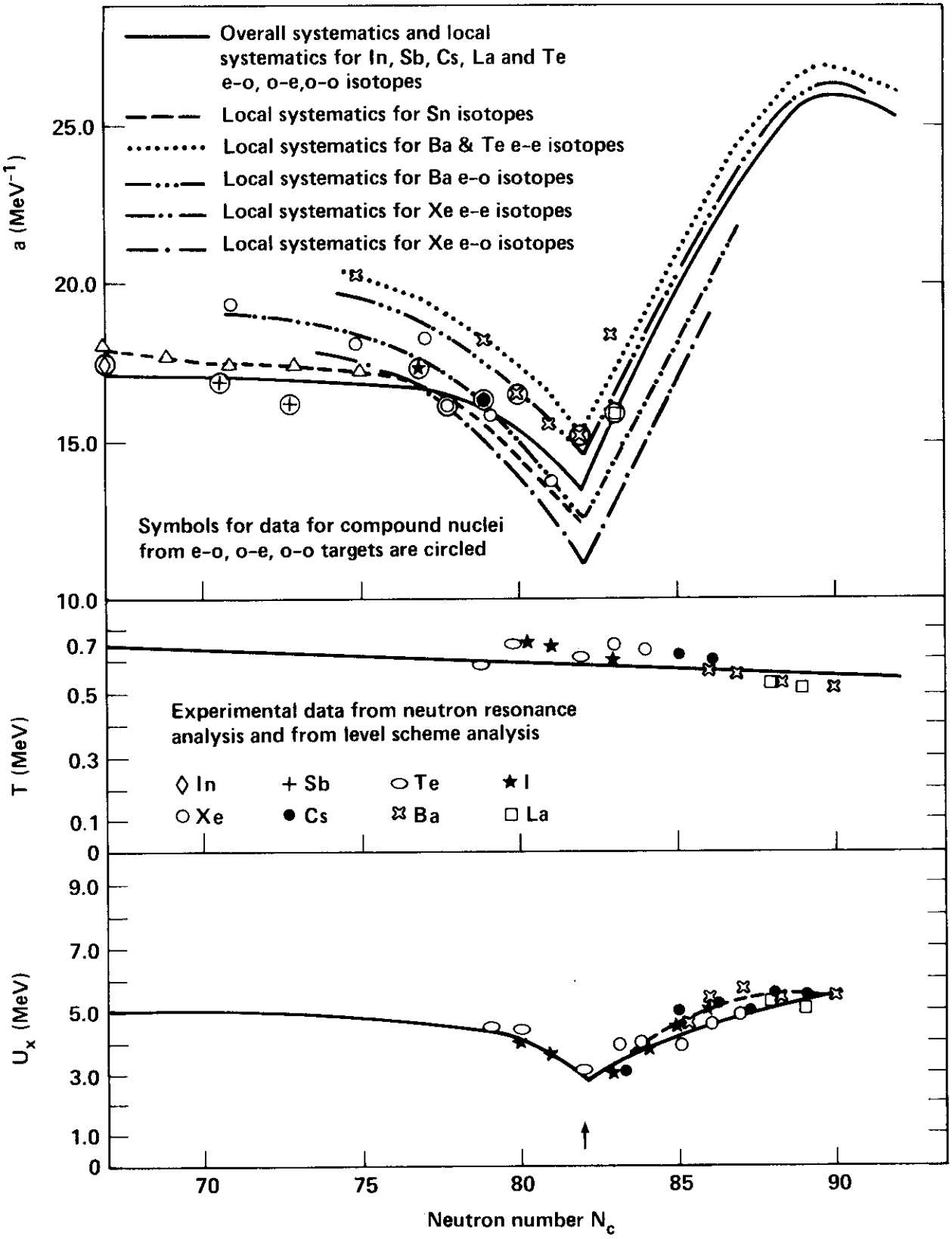
Overall systematics and local systematics for In, Sb, Cs, La and Te e-o, o-e,o-o isotopes
Local systematics for Sn isotopes
Local systematics for Ba & Te e-e isotopes
Local systematics for Ba e-o isotopes
Local systematics for Xe e-e isotopes
Local systematics for Xe e-o isotopes
a (MeV^{-1})
25.0
20.0
15.0
10.0
Symbols for data for compound nuclei from e-o, o-e, o-o targets are circled
T (MeV)
0.7
0.5
0.3
0.1
0
Experimental data from neutron resonance analysis and from level scheme analysis
◊ In
+ Sb
○ Te
★ I
○ Xe
● Cs
⊠ Ba
□ La
U_x (MeV)
9.0
7.0
5.0
3.0
1.0
0
70
75
80
85
90
Neutron number N_c

Figure 9

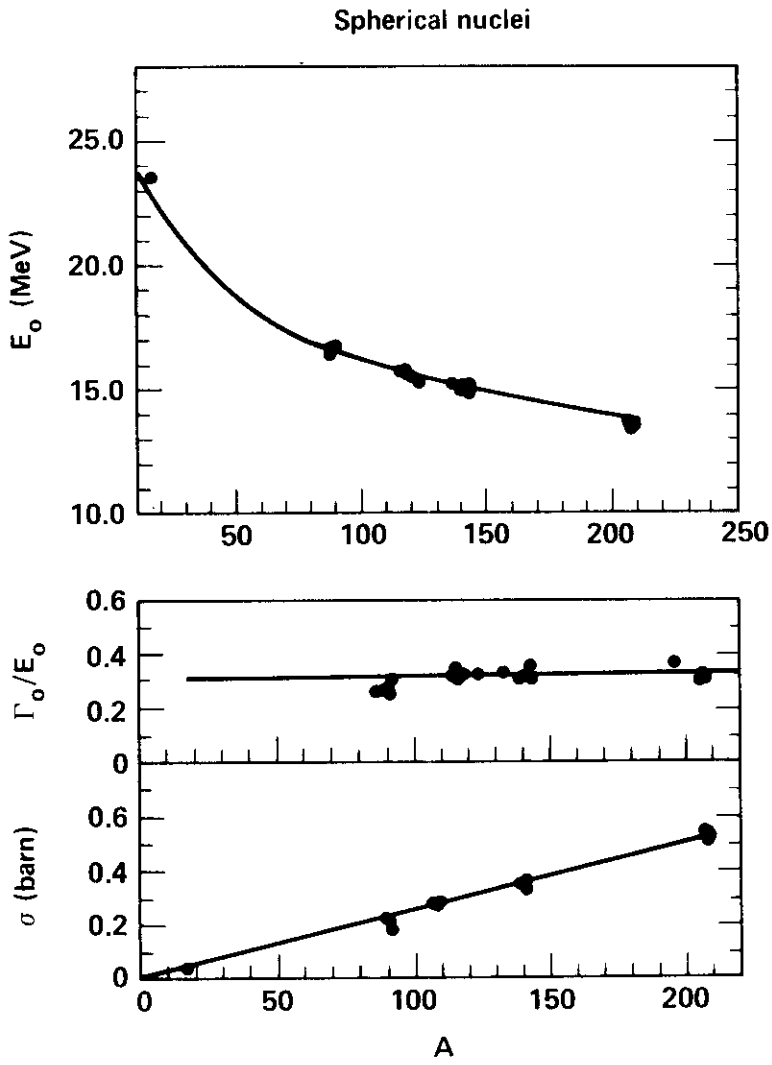
Spherical nuclei
25.0
20.0
15.0
10.0
E_o (MeV)
50
100
150
200
250
0.6
0.4
0.2
0
Γ_o/E_o
0.6
0.4
0.2
0
σ (barn)
0
50
100
150
200
A

Figure 10

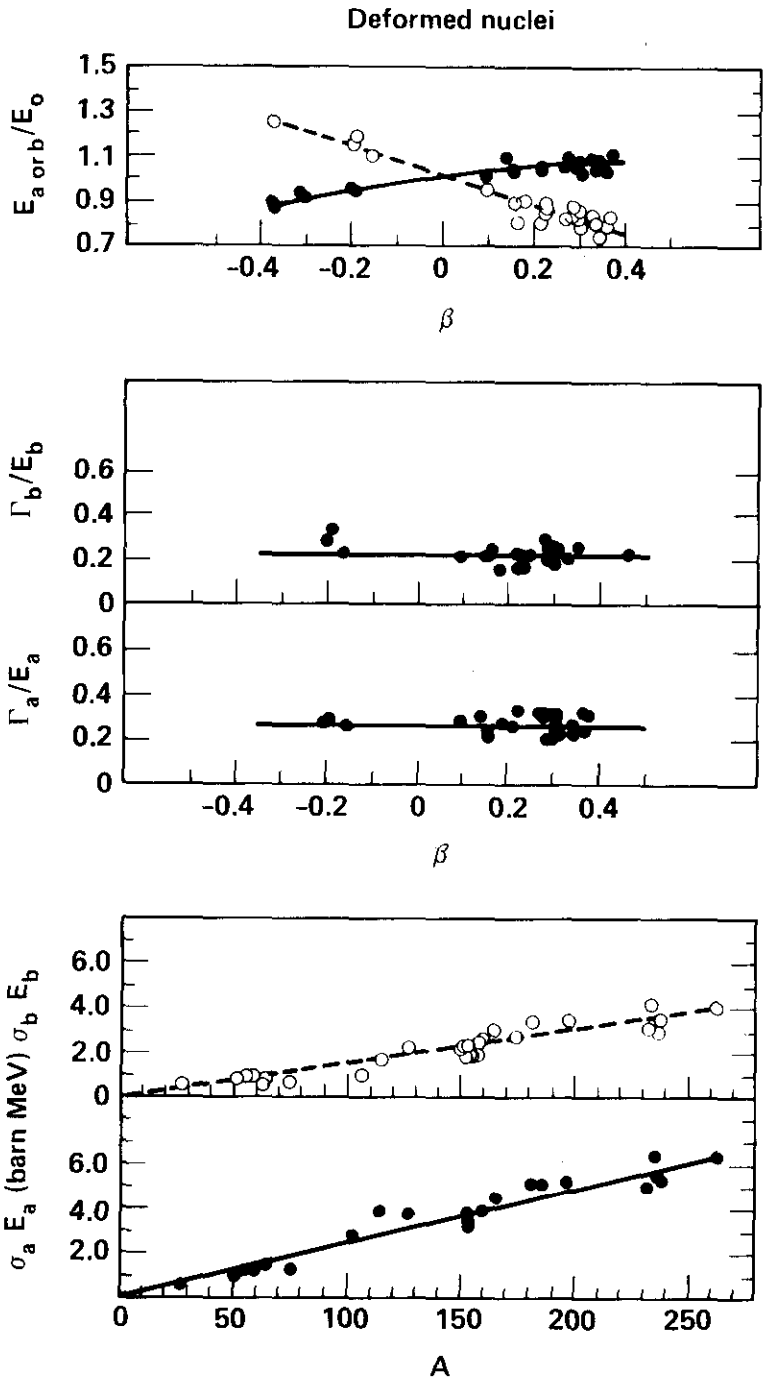
Deformed nuclei
$E_{a\,or\,b}/E_o$
1.5
1.3
1.1
0.9
0.7
-0.4
-0.2
0
0.2
0.4
β
Γ_b/E_b
Γ_a/E_a
0.6
0.4
0.2
0
$\sigma_a E_a$ (barn MeV) $\sigma_b E_b$
6.0
4.0
2.0
50
100
150
200
250
A

Figure 11

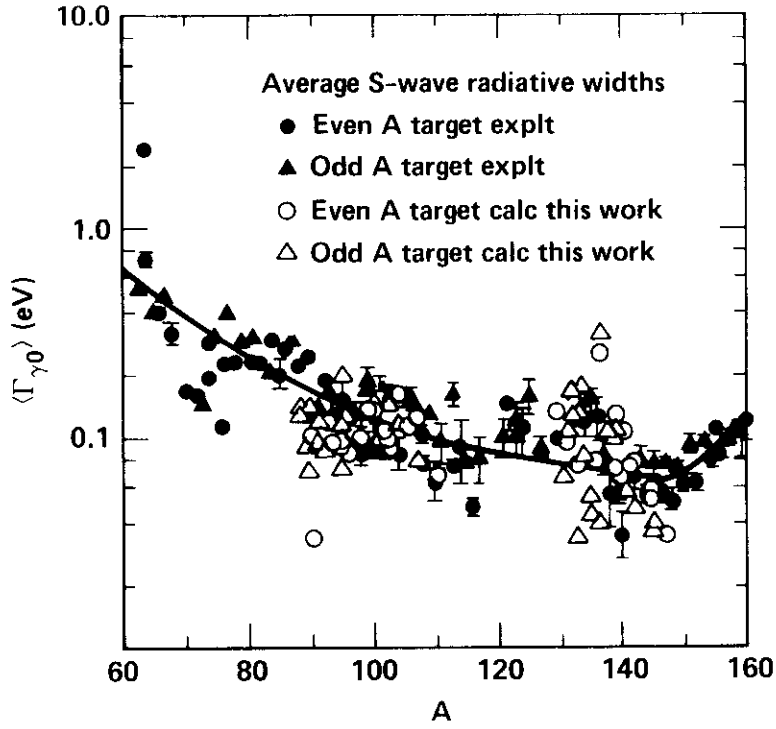
Average S-wave radiative widths
Even A target explt
Odd A target explt
Even A target calc this work
Odd A target calc this work
10.0
1.0
0.1
⟨Γγ0⟩ (eV)
60
80
100
120
140
160
A

Figure 12

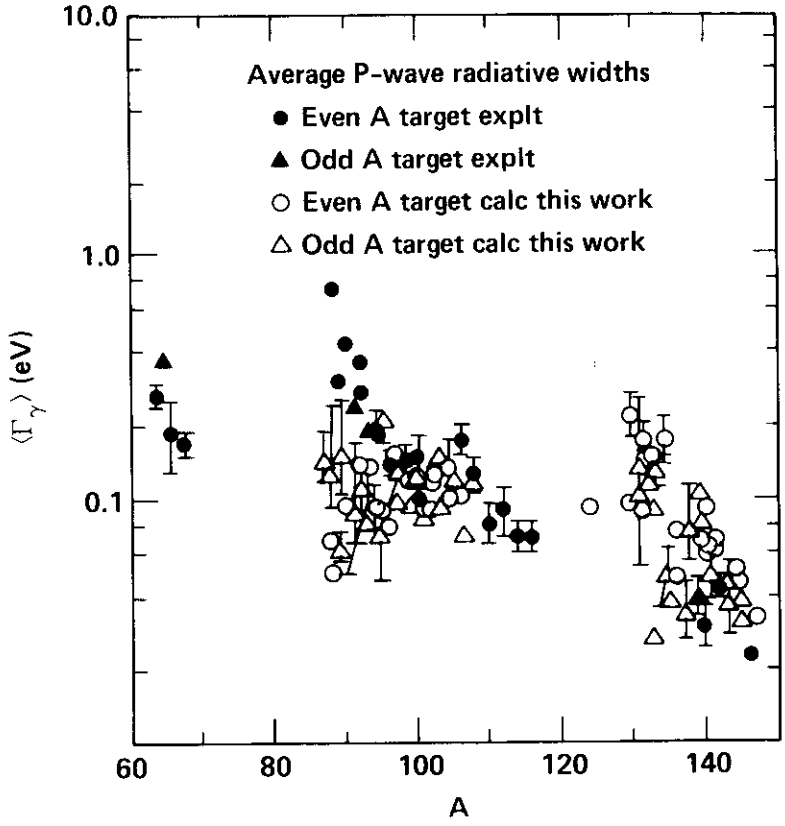
Average P-wave radiative widths
● Even A target explt
▲ Odd A target explt
○ Even A target calc this work
△ Odd A target calc this work
10.0
1.0
0.1
⟨Γγ⟩ (eV)
60
80
100
120
140
A

Figure 13